AD 645884

USAAVLABS TECHNICAL REPORT 66-4

HELICOPTER ROTOR NOISE GENERATION AND PROPAGATION

By

Robert Schlegel

Robert King

Harold Mull

October 1966

U. S. ARMY AVIATION MATERIEL LABORATORIES
FORT EUSTIS, VIRGINIA

CONTRACT DA 44-177-AMC-141(T)
SIKORSKY AIRCRAFT
DIVISION OF UNITED AIRCRAFT CORPORATION
STRATFORD, CONNECTICUT

Disclaimers

The findings in this report are not to be construed as an official Department of the Army position unless so designated by other authorized documents.

When Government drawings, specifications, or other data are used for any purpose other than in connection with a definitely related Government procurement operation, the United States Government thereby incurs no responsibility nor any obligation whatsoever; and the fact that the Government may have formulated, furnished, or in any way supplied the said drawings, specifications, or other data is not to be regarded by implication or otherwise as in any manner licensing the holder or any other person or corporation, or conveying any rights or permission, to manufacture, use, or sell any patented invention that may in any way be related thereto.

Disposition Instructions

Destroy this report when no longer needed. Do not return it to the originator.

This report has been reviewed by the U. S. Army

Aviation Materiel Laboratories and is considered

to be technically sound. This report is disseminated

for the exchange of information and the stimulation

of ideas.

Task 1P121401A14801

Contract DA 44-177-AMC-141 (T)
USAAVLABS Technical Report 66-4
October 1966

HELICOPTER ROTOR NOISE GENERATION
AND PROPAGATION

by

RONALD SCHLEGEL
ROBERT KING
HAROLD MULL.

Prepared by

Sikorsky Aircraft
Division of United Aircraft Corporation
Stratford, Connecticut

for

U. S. ARMY AVIATION MATERIEL LABOR. TORIES
FORT EUSTIS, VIRGINIA

SUMMARY

An improved method is presented for calculating rotor system over-all vortex noise and frequency spectra for stalled and unstalled rotors. Correlation of measured and predicted vortex noise was evaluated using two rotor systems operating over a wide range of speeds and thrusts. Correlation was found to be excellent. Blade tip planform studies revealed significant vortex noise reductions with tapered tips.

A new procedure is also derived for calculating near and far field rotor rotational noise with nonuniform inflow. The method extends the standard steady load method by including the effects of harmonic airloads. Correlation studies were conducted using an H-34 helicopter. Agreement between low frequency measured and predicted noise was good. However, correlation with high harmonic rotational noise was poor. This is probably due to inadequate definition of high harmonic airloads.

Presented results establish the importance of high harmonic rotational noise for detectability and loudness, and further work is recommended to more accurately define high harmonic blade loading. Since an airload measurement program is being conducted on the NH-3A, it is recommended that a correlation program be conducted to more fully evaluate the accuracy of the presented noise analysis program using the NH-3A airload results.

This study was performed for single rotor systems only, and in its present form is not directly applicable to systems with multiple rotors in juxtaposition.

FOREWORD

The program was conducted by Sikorsky Aircraft Division of United Aircraft Corporation under Contract DA 44-177-AMC-141 (T). USAAVLABS Project Engineer was Mr. J. McGarvey. The task was begun on 28 May 1964 and completed on 31 August 1965.

Acknowledgement is hereby made of the flight test data supplied by NASA Langley Research Center which supplement that published in NASA TM X-952. Personnel associated with the program were: Messrs. Kenneth C. Mard, Ronald G. Schlegel, Robert J. King, David C. Carmichael, Edward R. Wood, A. Charles Buffalano and Victor Berecz of Sikorsky Aircraft and Mr. H. R. Mull of H. R. Mull and Associates.

CONTENTS

CONTENTS (Con't)

ILLUSTRATIONS

FIGURE   PAGE

ix

ILLUSTRATIONS (Con't)

ILLUSTRATIONS (Con't)

TABLES

LIST OF SYMBOLS

A_B	blade area, square feet
a	blade chord, feet
b	blade thickness, feet
C_α	form drag coefficient
C_L	coefficient of lift
c	speed of sound, feet per second
d	diameter, feet
db	decibel
$\vec{F}$	force vector, pounds
$\vec{f'}$	arbitrary force per unit volume
f	frequency, cycles per second
g	Fourier coefficient
h	altitude, positive above rotor, feet
h'	projected blade thickness, feet
L	blade section loading, pounds per inch
M	Mach number
M_T	tip Mach number
m	order of harmonic
n	number of blades
P	pressure, pounds per square inch
p	sound pressure, pounds per square inch
p_m	sound pressure for mth harmonic, pounds per square inch

LIST OF SYMBOLS (Con't)

Q torque, pound-feet

R distance from center of rotor head to field point, feet

r distance from center of rotor head to source point in rotor disk, feet

r_T tip radius, feet

r_0 distance from center of rotor head to the point on the rotor blade where twist begins, feet

S distance from source point on rotor disk to field point, feet

SPL sound pressure level, decibels

S_t constant of value 0.28, Strouhal Number

T thrust, pounds

t time, seconds

ΔT time increment, seconds

u phase angle, radians

V velocity, feet per second

V_T velocity at tip, feet per second

W_α acoustic power, watts per square centimeter

x, y, z Cartesian coordinates (fixed system)

x_1, y_1, z_1 Cartesian coordinates in rotor system

α angle of attack, degrees

α_T angle of attack of tip, degrees

β blade pitch angle, radians

β_0 blade steady pitch angle at rotor head corresponding to collective pitch, radians

LIST OF SYMBOLS (Con't)

β_1 cosine component of cyclic pitch (ref: $\Upsilon = 0$), radians

$\overline{\beta_1}$ sine component of cyclic pitch (ref: $\Upsilon = 0$), radians

γ blade twist rate, radians per inch

θ field point azimuth angle, degrees

ζ blade chord location, feet

σ angle between rotor plane and field point - positive upward, degrees

Υ azimuth angle in rotor plane, degrees

Ω rotor rotational speed, radians per second

PHASE I

MAIN ROTOR VORTEX NOISE DURING UNIFORM INFLOW

INTRODUCTION

The task of Phase I was to develop an improved procedure for predicting single rotor helicopter main rotor vortex noise under conditions of uniform inflow. This task was accomplished by a review of vortex noise theory, development of a formula and a program of rotor stand measurements. Although the proposed work covered only the testing of one main rotor system under three conditions each of disk loading and rotor tip speed, the availability of another rotor system provided an opportunity to check analytical accuracy.

Previous studies of vortex noise generation by helicopter rotor systems have been limited to prediction of the overall levels for systems operating out of stall. Very little has been reported on prediction of the frequency spectrum for conditions either in or below stall. However, the importance of the spectral distribution of the noise in assessing the effects of rotor design on such psycho-acoustic factors as detectability and hearing damage requires the estimation of the spectrum shape. Consequently, the individual spectra were studied in detail.

This report presents the results of this study including an improved method of calculation of the noise levels and normalized spectra for operation in and out of stall. Sample spectra are given for both conditions. The improved method consists of corrections to Harvey Hubbard's formula (Reference 16) to account for changes in lift coefficient. The lift coefficient is now a variable, and the actual blade area is used rather than a calculated effective blade area. The coefficients to be used in this formula have been established empirically from CH-3C and CH-53A rotor test stand data.

VORTEX NOISE GENERATION

The subject of sound generation by fluid flow has been studied intensively by a number of investigators. Recent advances in the understanding of how sound is generated and propagated by unsteady aerodynamic phenomena such as vortices have permitted rigorous mathematical treatment. Reference 26 contains a complete physical and mathematical description of the phenomena of vortex sound.

1

Briefly, vortex sound is generated by the fluid force on an object arising from the formation and shedding of vortices in the flow past it. This results in a dipole form of radiation in which the strength of the source is proportional to the sixth power of the free-stream velocity.

For a rod or bluff body operating at low Reynolds numbers, the vortices are shed alternately from each side of the rod in regular vortex shedding. The shedding of vortices causes fluctuating lift and drag. The sound associated with the fluctuating drag is much weaker and is double the frequency of that associated with lift.

In the usual range of Reynolds numbers (approximately 5×10^6) associated with a rotating wing, the sound frequency is given by

$$f = S_t \frac{V}{d} \tag{1}$$

where V is the free-stream velocity and d is the thickness of the rod or bluff body. The Strouhal number, S_t, has been experimentally determined to have a value of 0.28 (Reference 28). Since there is a different velocity associated with each station over the span, there is a broad band of frequencies. However, the intensity of sound is proportional to the sixth power of the velocity V, so that the frequencies of interest are associated with the area near the tip where the velocity is highest. Table I shows the calculated frequencies and their relative intensity for the CH-53A rotor blade. From Table I, it can be seen that the most intense sound appears in the octave from 300 to 600 cps. For the purposes of this report, all of the sound from 150 to 9600 cps was considered to be vortex sound.

Although vortex sound is the principal source of medium and high frequency noise, boundary layer turbulence and noise from blade irregularities can contribute to the overall noise. Turbulence on the blade is another source of frequency broadening. The turbulence causes an irregular rate of shedding. If the blade is operating in a region beyond the onset of tip stall, there is a sharp rise in the 1200-to 2400-cps octave band associated with the flow separation in the region near the tip. This flow separation can be associated with blade slap as shown in Phase III.

CALCULATION OF VORTEX NOISE

Overall Level

A theory of vortex sound was first presented by E. Y. Yudin (Reference 33). Yudin's theory for the radiation of vortex sound from rotating rods was based on a dimensional analysis of the flow parameters around

2

the rods. In developing his theory, Yudin assumed that a rigid body in a moving fluid has forces impressed upon it due to the shedding of vortices. The sound radiation is the same in this case as that from equal but opposite forces acting directly on an otherwise still fluid.

Curle (Reference 4), in his analysis of the influence of solid boundaries on aerodynamic sound, showed that Yudin's result could be obtained formally from Lighthill's theory (Reference 19) in which the total fluid stress is associated with the local dipole strength. Curle has thus shown that Yudin's relationship was correct. Yudin's result can be written as follows:

$$ W_\alpha = const. \frac{\rho}{c^3} \left(C_\alpha^2 \, S_f \right)^2 V_T^6 \, r \, h' \qquad (2) $$

In using equation 2 to calculate vortex noise from rotating wings, some of the terms can be considered to be constant because their range of permissible values is too small to affect the results appreciably. These are ρ, c, C_α and S_f. Although C_α, the form drag coefficient, appears in the equation to the fourth power, the range in lift between an unloaded aircraft and a fully loaded aircraft is small enough to accept an average value for C_α for approximate calculations. Lumping the constant terms then gives the following:

$$ W_\alpha = const. \, V_T^6 \, r \, h' \qquad (3) $$

The two helicopter rotor systems tested had untapered 0012 airfoils. Therefore, a constant proportion exists between the chord and the thickness h'. Thus, the sound power is proportional to the chord length times the blade length r, or blade area. Furthermore, since the noise from each blade is additive, the total sound power will be proportional to the blade area of the rotor system. This simplifies the equation to the following:

$$ W_\alpha = const. \, A_B \, V_T^6 \qquad (4) $$

Equation 4 can now be compared directly to Hubbard's formula (Reference 16) which was used to calculate the sound pressure level of the vortex noise from propellers, which is as follows:

$$ SPL = 10 \log \left\{ \frac{K A_B (V_{0.7})^6}{10^{-16}} \right\} \qquad (5) $$

Hubbard's measurements were made at a distance of 300 feet and an angle of $105°$ from the axis of rotation. The constant K in equation 5 was determined empirically for the measurement position. The terms

3

10 log and 10^{-16} give the sound pressure level in decibels.

Hubbard's formula is based on $C_L = 0.4$. He adjusts the formula for other values of C_L by using an effective blade area, A_B. Intensive analysis of experimental rotor test data indicated that greater accuracy could be attained by using the actual blade area and coefficient of lift. The test data yielded a value of 6.1×10^{-27} for the constant K of equation 5 for use in a modified equation. Variations in lift for the modified equation are accounted for by addition of the term 20 log $C_L/0.4$ where the 0.4 is the coefficient of lift used by Hubbard in equation 5. The resulting equation is as follows:

$$SPL = 10 \log \frac{6.1 \times 10^{-27} A_B (V_{0.7})^6}{10^{-16}} + 20 \log \frac{C_L}{0.4} \qquad (6a)$$

This equation may be rewritten in a more convenient form for sea level 70°F conditions as follows:

$$SPL = 10\left\{2 \log V_{0.7} + 2 \log T - \log A_B - 3.57\right\} \qquad (6b)$$

Overall vortex noise levels were calculated for the CH-3C and CH-53A rotor systems by means of equations 5 and 6. The results of these calculations are shown in Table II. All numbers have been rounded off to the nearest db. As can be seen in Table II, the calculated levels agree with the measured levels within 2 db. Also, it can be seen that equation 5 is sufficiently accurate for all but the most stringent requirements.

Since equations 5 and 6 are for a distance of 300 feet from the center of rotation, the calculated values in Table II have been increased by 2.6 db to correct for the distance of 225 feet to the point of measurement. The usual distance corrections (20 log 300/R) can be made for distances other than 300 feet. *

Spectrum Shape

The spectrum shape of a blade operating out of stall is shown in Figure 19. This condition is present at low angles of attack at the tip. The peak frequency is determined by the Strouhal number which is defined as follows:

$$S_t = \frac{f h'}{V_{0.7}} \qquad (7)$$

In the usual range of Reynolds numbers for a helicopter rotor, the Strouhal number is 0.28. In keeping with Yudin's "round rod" approach,

* A sample calculation is shown in Appendix I.

4

the projected blade thickness h' is defined by the following equation:

$$h' = b \cos\alpha + a \sin\alpha \qquad (8)$$

where b is the blade thickness, a the chord length and α the angle of attack.

Tip Stall

When unsteady aerodynamic forces appear near the tip of a blade due to the occurrence of either stall or drag divergence, there is a definite change in the shape of the vortex noise level frequency spectrum. A portion of the rotor test data acquired was taken while portions of the blades were experiencing drag divergence (and probably stall as well), and the general spectrum obtained is shown in Figure 20. Compare this spectrum with that of Figure 19 where no separated flow is present and it is evident that the separated flow has caused a rise in the levels of the octaves above the peak octave. Using these curves (Figures 19 and 20), one may determine whether stall or drag divergence is present in a measured vortex noise spectrum. For prediction purposes, the proper spectrum may be selected on the basis of aerodynamic stall and drag-divergence criteria.

The exact point where tip stall begins is difficult to determine accurately. At that point, however, there is a deterioration of the lift/drag ratio. Figure 21 is a drag-divergence curve for the CH-3C blade. The experimental data points plotted indicated that some of the Mach number-angle of attack combinations are in the region of drag divergence.

In Figure 22 the difference between the 300 to 600 octave levels and the 1200 to 2400 octave levels is plotted against the blade tip pitch for the same data points of Figure 21. The rise of the 1200-to 2400-cps octave relative to the 300 to 600 octave corresponds with the data points that lie above the drag-divergence curves. The rise appears less abrupt for the high Mach numbers.

EXPERIMENTAL TEST PROGRAM

General

The object of the test program was to measure the vortex noise radiated by the rotor system over a range of speeds and loads. Two rotor systems were measured at three different speeds each and at several different thrusts at each speed. Test instrumentation is described in Appendix II.

Description of Rotor Systems

Both of the two systems tested used untapered 0012 airfoils and had square tips. The CH-3C system had five rotor blades and a diameter of 62 feet. The CH-53A system had six blades and a diameter of 72 feet. Although the program originally called for tests of only one rotor system, the opportunity to check the results with another quite different arrangement was valuable. The physical characteristics of each system are shown in Table III.

Acoustical Measurements

The rotors were tested on a whirl stand approximately 70 feet above the ground. Figure 1 shows the test arrangement. The ground plane around the test stand was covered with heavily matted dry grass except for a roadway. The microphone was mounted on a wire fence 225 feet to the east of the stand and about six feet above the ground.
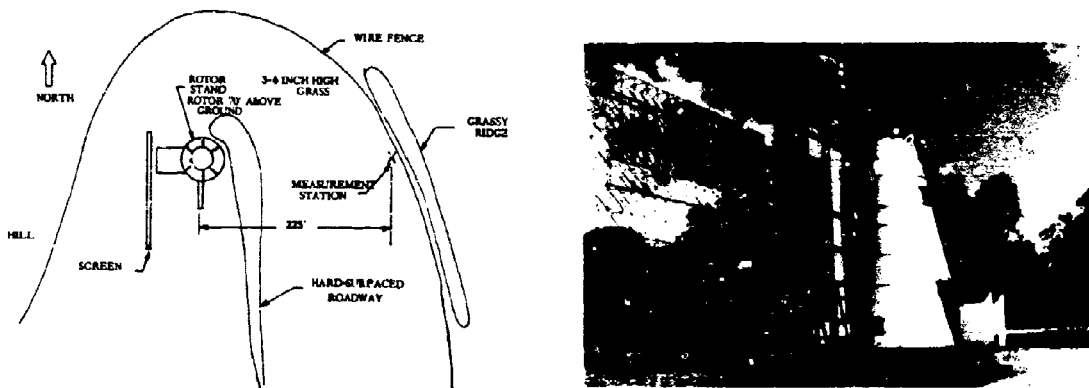

Figure 1. Vortex Noise Test Arrangement and Rotor Test Stand

There was a grassy ridge beyond the fence and a wooded hill to the west of the stand. All measurements were made at the same microphone position. It is assumed that the measurements were the direct field from the test rotor because (1) the portion of the spectrum of interest was above 150 cps, (2) the test rotor was 70 feet above the ground, and (3) the ground was covered with an absorbent grass cover.

Since the sound fields are strongly affected by winds, measurements were made when the ambient wind was below 5 knots. Thus the measured data should closely approximate free field conditions unaffected by non-uniform inflow.

PHASE II

HELICOPTER ROTATIONAL NOISE UNDER CONDITIONS OF

NONUNIFORM INFLOW

INTRODUCTION

Rotational noise, which is comprised of discrete frequencies at multiples of the blade passage frequency, as opposed to vortex noise, which is broad-band random noise centered about the Strouhal frequency, was first defined by Gutin (Reference 11) in 1948. Since the establishment by Gutin's theory, there have been a number of outstanding studies (References 1, 7, 14, 17, 30, 34) involving propeller rotational noise generation and propagation. These studies have extended the rotational noise theory developed by Gutin to account for noise in the near field, thickness noise, and noise field distortion due to source translational motion. It is desirable to make use of the techniques developed through these studies to obtain increased accuracy where Gutin's model is found to be inadequate.

The study undertaken here has followed along the lines of those mentioned above in that it seeks to extend Gutin's basic theory for noise generated by a particular type of propeller, in this case the helicopter rotor. Gutin's theory is still commonly used for propeller noise prediction but is subject to the following limitations:

1. Uniform axial inflow is maintained throughout the propeller disk.
2. Field points, at least 5 diameters from the hub, are calculated (far field).
3. Only first harmonic noise is calculated.
4. Propeller speed normal to the axis is held below approximately Mach 0.3.

In the case of the helicopters, the inadequacy of Gutin's theory is obvious; diameters are large and inflow is nonuniform because of predominantly nonaxial translational motion. Most rotor noise field points of interest fall within the "near field", and generally the first rotational noise harmonic falls below the audible frequency range, making it less important than its harmonics.

In general, the intensity of these harmonics cannot be predicted accurately. This report represents a newly developed mathematical theory which removed the limitations of Gutin's theory as applied to the rotational noise of single rotor helicopters.

The prediction method utilizes blade section loading, both steady and varying at integral multiples of the main rotor rotational speed, as a function of radius and azimuth. The solution describes as many harmonics of rotational noise as the input data allows in both the near and far field. The periodically varying blade loading comprises the variable inflow condition. This solution has been programmed by Sikorsky Aircraft as an IBM-7094 procedure.

DERIVATION OF VARIABLE INFLOW ROTATIONAL NOISE SOLUTION

The rotor system noise source will be represented by a surface of stationary dipole radiators which simulate the normal pressure distribution in the rotor disk. Shear forces as well as thickness effects are ignored. It can be shown (References 7 and 18) that for sound sources in rectilinear motion, the acoustic pressure in the sound field can be exactly represented by the sum of pressure from stationary sound sources placed in the path of the moving source which radiate only when the moving source passes by. In this case the stationary sound sources are the dipoles in the rotor disk which radiate only when a blade (corresponding to the moving source) passes by.

Solution of Wave Equation

For the range of rotational Mach numbers and sound frequencies considered here, the pressure field due to a rotating force is the sum of pressure fields from stationary dipoles, and the radiation from the stationary dipoles satisfies the nonhomogeneous wave equation

$$\nabla^2 p - \frac{1}{c^2}\left\{\frac{\partial^2 p}{\partial t^2}\right\} = \nabla \cdot \vec{f} \tag{9}$$

where $\vec{f}$ is an arbitrary force per unit volume.

Since this wave equation is for radiation from a stationary force into a stationary medium, it is exact for only hover conditions. However, as long as the vehicle translational Mach number is below 0.3, the accuracy of the wave equation is considered adequate, as shown in Reference 23.

Figures 2 and 3 show the geometry of the rotor system used in the analysis and the sound field coordinate system. The force vectors $\vec{F}(r, \psi, t)$ are restricted to the region covered by the rotor disk, and the field point is outside of a sphere having the diameter of the rotor disk and centered at the rotor hub.

8

The solution to equation 9 for concentrated forces is given by

$$P(x,y,z,t) = -\frac{1}{4\pi} \, div \left[\frac{\vec{F}(S,\theta,\sigma,t-\frac{S}{c})}{S} \right] \tag{10}$$

where

$$S = \sqrt{(x-x_i)^2 + (y-y_i)^2 + (z-z_i)^2}$$

is the distance from the elemental source point to the field point.

Since the forces of interest here are harmonic at integral multiples of the rotor blade passage, the force vector may be represented by a Fourier series:

$$\vec{F}(r,\psi,t) = \sum_{m=1}^{\infty} \vec{g}_m(r,\psi) \, e^{imn\Omega t} \tag{11}$$

where the steady component is neglected because it is not an acoustic signal. The component of the vector $\vec{F}$ in the X direction is

$$F_x(r,\psi,t) = \sum_{m=1}^{\infty} g_{mx}(r,\psi) \, e^{imn\Omega t}$$

where $g_{mx}(r,\psi)$ is the component of $\vec{g}_m(r,\psi)$ in the X direction. Similar components exist in the y and z directions.

Using these expressions in equation 10 yields

$$P(x,y,z,t) = -\frac{1}{4\pi} \left\{ \frac{\partial}{\partial x} \frac{1}{S} \sum_{m=1}^{\infty} g_{mx} \, e^{i(mn\Omega t - mn\Omega \frac{S}{c})} + \right.$$

$$\frac{\partial}{\partial y} \frac{1}{S} \sum_{m=1}^{\infty} g_{my} \, e^{i(mn\Omega t - mn\Omega \frac{S}{c})} +$$

$$\left. \frac{\partial}{\partial z} \frac{1}{S} \sum_{m=1}^{\infty} g_{mz} \, e^{i(mn\Omega t - mn\Omega \frac{S}{c})} \right\} \tag{12}$$

9
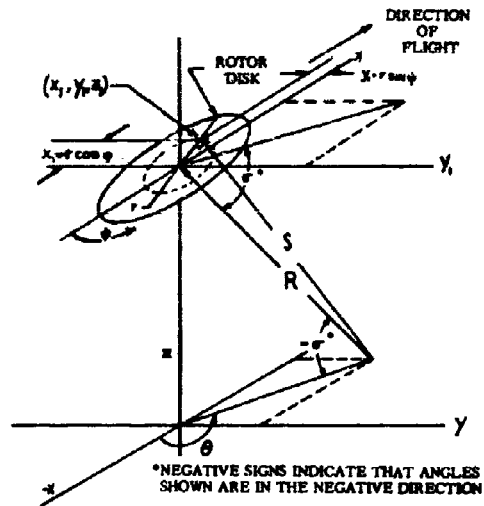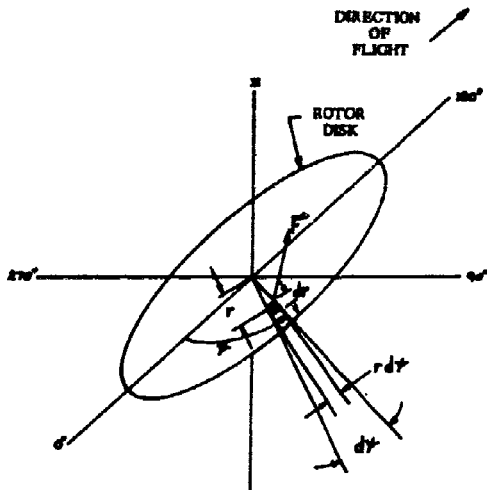
Figure 2. Rotor System Geometry   Figure 3. Field Point Location

which reduces to

$$p(x,y,z,t) = -\frac{1}{4\pi}\sum_{m=1}^{\infty} e^{imn\Omega t}\left\{ g_{mx}\left(\frac{\partial S}{\partial x}\right) + g_{my}\left(\frac{\partial S}{\partial y}\right) + g_{mz}\left(\frac{\partial S}{\partial z}\right)\right\}\frac{\partial}{\partial S}\left(\frac{e^{-imn\Omega\frac{S}{c}}}{S}\right) \tag{13}$$

This expression describes the sound pressure $p(x,y,z,t)$ at the field point x, y, z at time t due to the force components g_{mx}, g_{my}, g_{mz} acting at the point r, ψ in the rotor disk. Now the components of equation 13 are defined.

As previously defined

$$S = \sqrt{(x-x_1)^2 + (y-y_1)^2 + (z-z_1)^2}$$

which in spherical coordinates (Figure 3) is

$$S = \sqrt{(R\cos\sigma\cos\theta + r\cos\psi)^2 + (R\cos\sigma\sin\theta - r\sin\psi)^2 + (R\sin\sigma)^2}$$

10

which reduces to

$$S = \sqrt{R^2 + r^2 - 2rR\cos\sigma\cos(\theta - \psi)} \tag{14}$$

This is an exact representation and holds for both near and far field. From Appendix III

$$\frac{\partial S}{\partial x} \approx -\frac{R}{S}\cos\sigma\cos\theta$$

$$\frac{\partial S}{\partial y} \approx \frac{R}{S}\cos\sigma\sin\theta$$

$$\frac{\partial S}{\partial z} \approx \frac{R}{S}\sin\sigma \tag{15}$$

Equation 15 is valid outside of one rotor diameter from the hub.

The differential

$$\frac{\partial}{\partial S}\left\{\frac{e^{-imn\Omega\frac{S}{c}}}{S}\right\}$$

becomes

$$-\left\{\frac{1}{S} + \frac{imn\Omega}{c}\right\}\frac{e^{-imn\Omega\frac{S}{c}}}{S} \tag{16}$$

Placing equations 15 and 16 into equation 13 yields for the harmonic m

$$P_m(x,y,z,t) = \frac{R}{4\pi S^2}\,e^{imn\Omega\left(t - \frac{S}{c}\right)}\left[-g_{mx}\cos\sigma\cos\theta + g_{my}\cos\sigma\sin\theta + g_{mz}\sin\sigma\right\}\left\{\frac{imn\Omega}{c} + \frac{1}{S}\right\} \tag{17}$$

Now the forces g_{mx}, g_{my}, g_{mz} acting on the rotor blade remain to be determined.

Blade Aerodynamic Loads

Blade pressures for this study were obtained from flight test measurements taken on a Sikorsky S-58 (Army CH-34) at NASA, Langley Field, Virginia (Reference 29). This data consists of differential pressure measurements made on one main rotor blade during various flight

11

conditions. Data was recorded at several chordal stations and integrated over the chord at 15-degree azimuth intervals, yielding section loadings at these points. This was done at several blade spanwise stations. At each station, a harmonic analysis was performed on the section loading-azimuth position curve resulting in a steady plus 10 harmonics of the loading. This harmonic blade loading data is utilized for the present study.

Transformation of Rotating Concentrated Forces to Stationary Forces

Consider a rotating blade with a normal differential pressure distribution given by $\Delta P(r, \zeta, t)$ and located as shown in Figure 4.
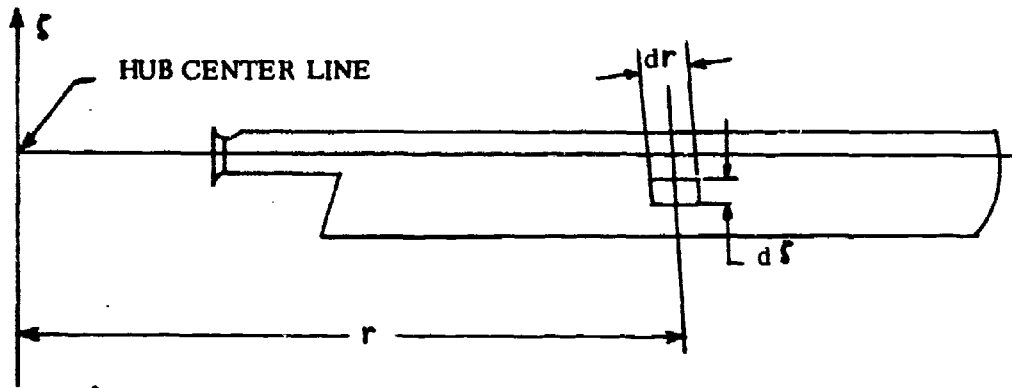
Figure 4. Blade Normal Differential Pressure Location

The force acting on a small blade area is $\Delta P d\zeta dr$ and is considered to be concentrated force when $d\zeta dr$ is very small. This same force will be considered to be acting on a differential area at the rotor disk $r dr d\psi$ when the blade area is covering the rotor disk area (Figure 2). The time history of pressure as two blades pass over the area $r dr d\psi$ is shown in Figure 5.
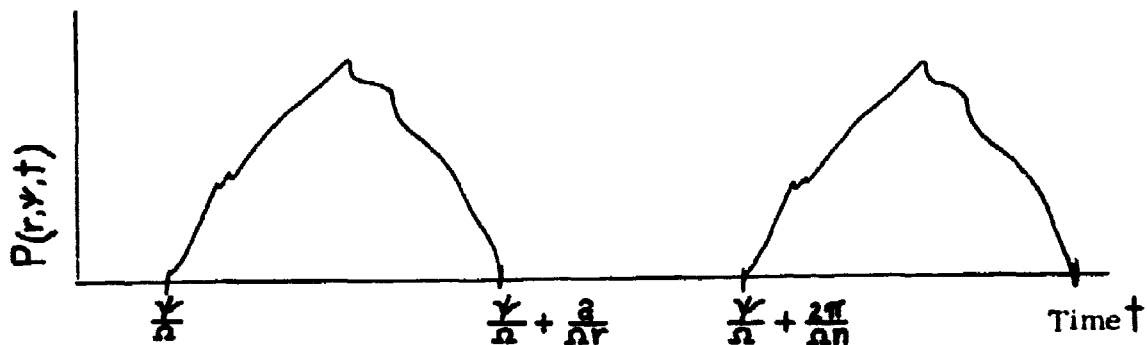
Figure 5. Pressure Time History of Blade Passing Over an Elemental Disk Area

12

Note that the only time a pressure exists is when a blade covers the area. The amount of time an elemental area is covered is finite and equal to the time it takes for the blade to pass a given point. That is $\Delta T = a/\Omega r$. The time between blades is equal to the time required for a blade to traverse $2\pi/n$ radians or $\Delta T = 2\pi/n\Omega$. The magnitude of the force acting on the rotor disk is $\Delta P r dr d\psi$ and its direction is normal to the chord. After shifting scale and approximating the chordwise pressure distribution as a step function (see Appendix IV), the function of Figure 6 is obtained.

$$\overline{\Delta P}(r, \psi)$$

$$\frac{-a}{2\Omega r} \qquad 0 \qquad \frac{a}{2\Omega r} \qquad \text{Time } t$$
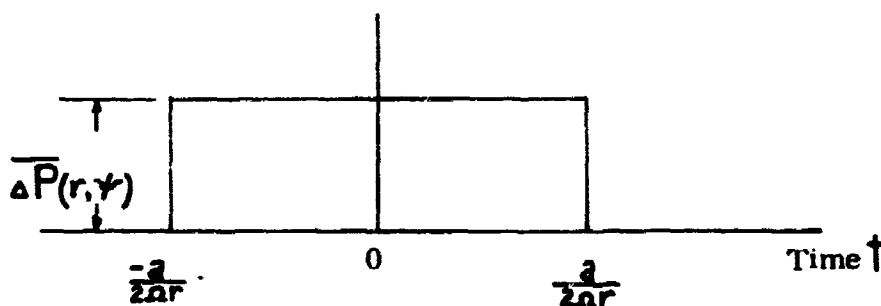
Figure 6. Step Function

The cosine series expansion of this function is

$$\Delta P(r, \psi, t) = \sum_{m=1}^{\infty} a_m \cos\left(mn\Omega t - mn\psi - \frac{man}{2r}\right) \qquad (18)$$

where

$$a_m = \frac{2}{mn} \sin\left(\frac{man}{2r}\right) \overline{\Delta P}(r, \psi) \qquad (19)$$

and $\overline{\Delta P}$ is the average chordal pressure on the blade.

Since average pressure data is available (Reference 29) as blade loading data $L(r, \psi)$ and

$$L(r, \psi) = a \overline{\Delta P}$$

equation 19 becomes

$$a_m = \frac{2}{mn\pi a} \sin\left(\frac{man}{2r}\right) L(r, \psi) \qquad (20)$$

13

Substituting 20 into 18 yields:

$$\Delta P(r,\Psi,t) = \sum_{m=1}^{\infty} \frac{2}{m\pi a} \sin\left(\frac{man}{2r}\right) L(r,\Psi) \cos\left(mn\Omega t - mn\Psi - \frac{man}{2r}\right) \quad (21)$$

Putting this into complex form and multiplying by $r\,dr\,d\Psi$ to change to force yields

$$F(r,\Psi,t) = \sum_{m=1}^{\infty} \frac{2}{m\pi a} \sin\left(\frac{man}{2r}\right) L(r,\Psi)\, e^{i\left(mn\Omega t - mn\Psi - \frac{man}{2r}\right)} r\,dr\,d\Psi \quad (22a)$$

and from Equation 11

$$g_m = \frac{2}{m\pi a} \sin\left(\frac{man}{2r}\right) L(r,\Psi)\, e^{-imn\left(\Psi + \frac{a}{2r}\right)} r\,dr\,d\Psi \quad (22b)$$

Figure 7. Aerodynamic Forces Generated by a Blade

Equation 22 corresponds to the force exerted on the rotor disk by a passing blade in the direction normal to the blade chord. From Figure 7, note that the out-of-plane component of $\vec{g_m}$ is

$$g_{mz} = g_m \cos\beta \quad (23a)$$

and from Figures 2 and 7 the in-plane components are

$$-g_{mx} = g_m \sin\beta \sin\Psi \quad (23b)$$

$$-g_{my} = g_m \sin\beta \cos\Psi \quad (23c)$$

where

$$\beta = \beta_0 - \gamma(r - r_0) + \beta_1 \cos\Psi + \overline{\beta_1}\sin\Psi$$

as derived in Appendix V.

Substituting equation 22 into equation 23 and substituting the result in equation 17 gives

$$P_m(x,y,z,t) = e^{imn\Omega t}\left\{\frac{R}{2\pi^2 am}\frac{L(r,\Psi)}{S^2}\sin\left(\frac{man}{2r}\right)\right\} e^{-imn\left(\frac{\Omega S}{c} + \Psi + \frac{a}{2r}\right)} \quad (24)$$

$$\left\{\frac{imn\Omega}{c} + \frac{1}{S}\right\}\left\{\sin\beta \sin\Psi \cos\theta \cos\sigma - \sin\beta \cos\Psi\cos\sigma\sin\theta + \cos\beta \sin\sigma \right\} r\,dr\,d\Psi\right\}$$

14

This expression after integrating, transforming to the uniform disk loading case, and introducing the small angle assumptions made in References 11 and 7, reduces to the sum of equations 21 and 22 of Reference 7 for Mach zero. It represents the sound pressure at a point x, y, z, at time t of the m'th harmonic of rotational noise due to the blade section loading $L(r, \psi)$ on the radius r of the blade when the blade is at azimuth location ψ. The equation may be integrated over the rotor disk to account for all sources and the root mean square (rms) value of the pressure with respect to time may be taken to correlate with sound pressure measurements. These operations result in the following solution:

$$P_{rms} = \frac{1}{\sqrt{2}} |P_m| = \frac{1}{\sqrt{2}} \left\{ P_{re}^2 + P_{im}^2 \right\}^{\frac{1}{2}} \tag{25}$$

$$P_{rms} = \frac{R}{2\sqrt{2}\,\pi^2 a} \left\{ (P_{re}')^2 + (P_{im}')^2 \right\}^{\frac{1}{2}} \tag{26a}$$

where

$$P_{re}' = \int_0^{2\pi} \int_0^{r_t} \frac{L(r,\psi)}{mS^2} \sin\left(\frac{man}{2r}\right) \left\{ \frac{mn\Omega}{c} \sin u + \frac{\cos u}{S} \right\}$$

$$\left\{ \sin\beta \cos\sigma \sin(\psi-\theta) + \cos\beta \sin\sigma \right\} r\, dr\, d\psi \tag{26b}$$

$$P_{im}' = \int_0^{2\pi} \int_0^{r_t} \frac{L(r,\psi)}{mS^2} \sin\left(\frac{man}{2r}\right) \left\{ \frac{mn\Omega}{c} \cos u - \frac{\sin u}{S} \right\}$$

$$\left\{ \sin\beta \cos\sigma \sin(\psi-\theta) + \cos\beta \sin\sigma \right\} r\, dr\, d\psi \tag{26c}$$

for which

$$u = mn\left\{ \frac{\Omega S}{c} + \frac{a}{2r} + \psi \right\}$$

This integral solution (equation 26) represents the rms sound pressure at a point x, y, z for rotational noise at the m'th harmonic of blade passage. This solution may be used for calculating the rms sound pressure at any point in the near or far field one diameter or more from the rotor hub. The number of harmonics which may be calculated accurately is limited only by the detail of the available blade loading data. The solution's accuracy decreases with increasing rotor system translational speed up to Mach 0.3, which is the practical limit for accuracy.

The solution has been programed as an IBM-7094 procedure to facilitate calculation. The program is described in Appendix VI.

A trial case was run with steady loads only placed about the 0.8 radius point of the rotor as assumed in Gutin's derivation (Reference 11).

Using relationships between blade pitch, loading, radius, etc., the torque and thrust for this case were calculated for the S-58 rotor system. The derivation is explained and parameters for the example are given in Appendix VII. Calculations of first harmonic noise were made at a 320-foot radius by both the Sikorsky program and by Gutin's equation for various elevation angles. The results of these calculations are tabulated in Table IV and shown in Figure 8.

Agreement between the two solutions is excellent except for the point where σ is -30 degrees. At this spatial point, Gutin's solution involves a small difference between two large numbers, and the number of significant digits used in the hand calculation was not sufficient to define the true magnitude.

To further check the solution's validity, a similar calculation was made comparing the program output with the near field case (Figure 4 of Garrick and Watkins, Reference 7). The comparison is shown in Figure 9 for zero Mach number.

Figure 8. Comparison of Sikorsky Program and Gutin Equation Results at 320-Foot Radius

x/d IN FIELD POINT PLANE
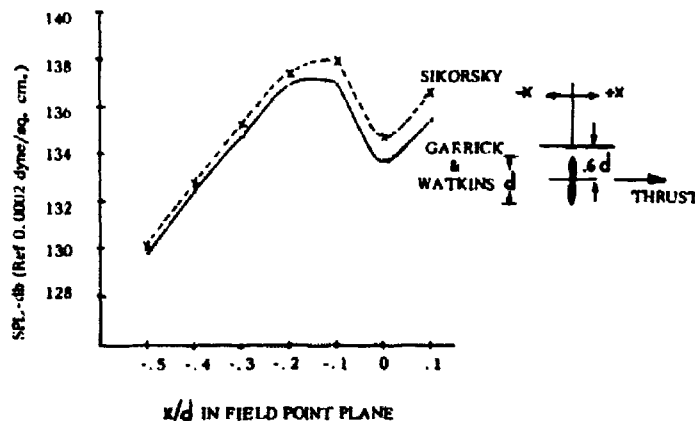
Figure 9. Comparison of Results From Developed Solution and Garrick and Watkins' Results

16

The agreement between the calculated values and those of Garrick and Watkins is excellent, the maximum deviation being 1 db up to 1/2 diameter downstream of the propeller.

EXPERIMENTAL TEST PROGRAM

General

Measurements of rotational noise from an S-58 (CH-34) helicopter were made at Bridgeport Airport in Stratford, Connecticut, on April 5, 1965. Physical and test parameters of the aircraft are listed in Table V. Instrumentation is described in Appendix VIII. The purpose of the test was to provide data for comparison with the calculated data of Phase II. It was found during testing that although rotor noise harmonics up to the tenth were sometimes distinguishable above background noise, harmonics above the fourth (approximately 60 cps) were generally masked by engine and tail rotor noise.

Description of Test Helicopter

The S-58 (Figure 10) is a single main rotor reciprocating engine helicopter in the 13,000-pound weight class. The main rotor is 4 bladed, with 0012 airfoil shape and untapered square tip blades.

Figure 10. S-58 Helicopter

17

Acoustical Measurements

The test layout is shown in Figure 1.
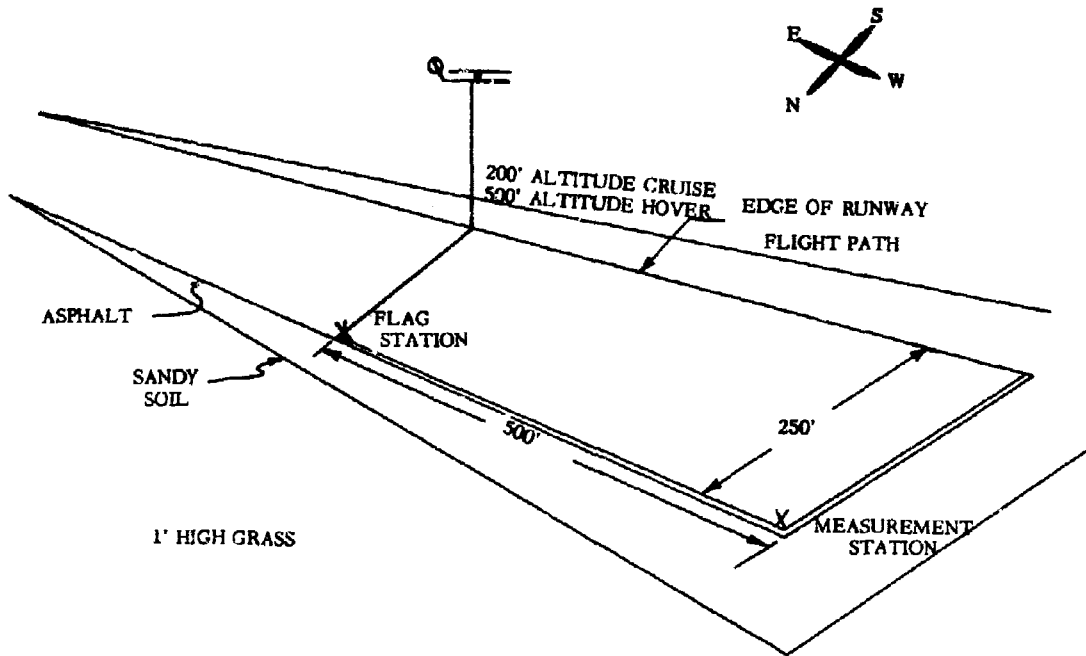
Figure 11.   Rotational Noise Test Layout

The ambient wind was northeasterly at approximately 4 miles per hour, gusting occasionally to 10 miles per hour.   The flight path for cruise measurements was from east to west directly over the south edge of the runway.   The ship's altitude was 200 feet for all cruise and transient measurements.

For a time and location reference, a flag was dropped as the ship passed the flag station, signalling the measurement station to put a short-duration 400-cycle-per-second signal tone on the recording tape. Using the aircraft's indicated airspeed, its position was calculated from this signal. One-third-octave band analysis was used and the frequencies under study went only up to 60 cps, thereby eliminating the possibility of the 400-cps tone interfering with the records.

Because the noise was a series of pure tones, actual bandwidth was not important in determining levels. One-third-octave filters were used so as to define the individual harmonics and to accommodate the doppler shift for the flyby conditions.

18

Because of safety regulations, hover measurements were made at an altitude of 500 feet. The hover location was above the south edge of the runway.

Data was recorded with the microphone held approximately three feet above the ground. The runway between the aircraft and microphone was hard-surfaced. In the frequency range of interest, 15 to 60 cps, the wavelength of 75 to 18 feet precluded interference or reinforcement between the incident and reflected waves.

Noise data was recorded for hover; 40-knot, 80-knot, and 110-knot cruise; and 70-knot cyclic pullout. These conditions correspond to the blade loading data of Reference 28 (Tables 4, 8, 13, 19, and 111, respectively).

CORRELATION OF MEASURED AND CALCULATED ROTATIONAL NOISE

Correlation of measured and calculated rotational noise levels is summarized for the first harmonic in Table VI. The calculated levels shown are the maximum attained for flybys using NASA (Reference 29) blade loading data. The measured levels are the corresponding maximums for the test flybys. The blade loading tables from Reference 29 which were used are listed in Table VII. The spread of data for the measured hover condition is due to time variation. Levels calculated by Gutin's equation, using thrusts and torques as shown for the S-58, are included for reference. Note that the calculated and measured levels agree within 3 db, while Gutin's equation gives levels as much as 19 db low. Gutin's method is most nearly accurate (3 db low) during hover where the inflow is almost uniform. Obviously, nonuniform inflow has a significant effect on rotor first harmonic noise levels. The effect of nonuniform inflow is even more pronounced for the higher noise harmonics. The conclusion is that Gutin's equation is not an adequate method of predicting rotor noise levels during nonuniform inflow.

Figure 23 shows calculated and measured levels for a 500-foot hover. The program calculated the measured data much more closely than Gutin's equation, which predicts a rapid dropoff in level with increasing harmonic.

It is felt that the agreement between the calculated and measured levels for the higher harmonics would have been closer than that shown if the flight test conditions under which the noise measurements were made were identical with those for which the blade loading data was taken. According to Reference 29, the blade loading test aircraft was "hovering in light wind", which implies slight, relatively steady wind

19

conditions, while during the noise measurement test, winds ranged from 4 to 10 knots. The lack of agreement between the measured and calculated levels for the higher harmonics can be attributed partly to the uncertainty in blade loading harmonics caused by the variable wind velocity.

Levels for the cruise and transient flybys are shown in Figures 24 through 27. As shown, the data is 1-1/2 db low at the plus 250-foot and minus 250-foot points. This error results from the frequency change due to doppler effects reaching the band limits of the one-third-octave filter used in the analysis. Correlation of measured and calculated data is good for the first two harmonics. It appears for some of the cases that the distance scale is shifted. This may be attributed partially to lag in the time reference system used in the test and partially to uncertainty as to the test aircraft's ground speed.

Agreement between the third and fourth harmonics, and presumably for all higher harmonics, is poor. This can be attributed to differences in flight conditions between blade loading test and noise test, as mentioned earlier, and to the lack of sufficient higher harmonic content in the NASA blade loading data (Reference 29). Blade loading containing a greater proportion of higher harmonics would yield more nearly accurate higher harmonics of noise as explained in Phase III.

The observed chordal loading distribution for the data used in this report conforms to the general shape of Figure 12, which yields a harmonic level distribution similar to that of the rectangular distribution used. It should be noted that if the blade chordal pressure distribution had exhibited the form of the one shown in Figure 13, the rectangular chordal pressure distribution used in the program would yield much lower noise harmonic levels than actually exist. For all common cases of propeller or rotor loading where forces on the disk act in one direction, the assumption of uniform loading over the chord should yield realistic values for calculated noise. The effects of variation in chordal loading are treated in detail in Reference 31.
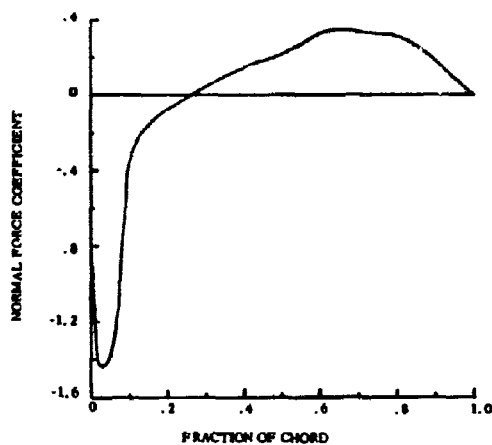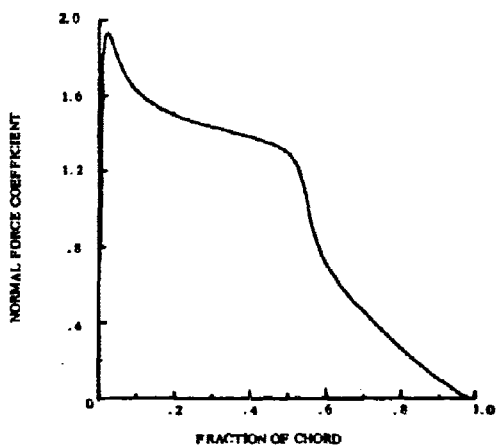
Figure 12. Chordwise Normal Force Figure 13. Chordwise Normal Force
Distribution   Distribution With Reverse Flow

APPLICATIONS OF THE ROTATIONAL NOISE SOLUTION

The theory derived here for rotational noise generation lends itself
to the evaluation of rotor design parameters better than the classical
theory (Reference 11) for conditions of uniform inflow. For the more
significant condition of nonuniform inflow it becomes a unique tool for
study. The drawback is that the correct harmonic blade loading is
required as input, and this is not available for harmonics above the
fifth. Analysis (References 8 and 32) is available to calculate these
blade loadings; however, the rotor inflow (References 21, 24, and 25) is
not known in sufficient detail to allow the calculations to be made. Lack
of information regarding blade wake geometry is the problem in predict-
ing rotor inflow characteristics. The importance of the need for higher
harmonic blade loading cannot be overemphasized, as the usefulness of
the rotational noise solution depends on further progress in this area.
In the case where some blade loading harmonics are known, even if only
hand calculated steady loads, the distortion of the classical propeller
noise field (Reference 11) due to planform, twist, blade collective,and
cyclic pitch can be calculated in both the near and far fields. The effects
of any other parameter changes are easily dealt with if blade loadings are
known. Note that the solution, in its present form, is not directly appli-
cable to systems with multiple rotors in juxtaposition.

21

PHASE III

ROTOR DESIGN TECHNIQUES FOR ALLEVIATION OF NOISE

VORTEX NOISE REDUCTION

The research in Phase I has shown how rotor vortex noise is generated and propagated. The theory developed permits accurate prediction of the noise amplitude and frequency spectrum directly from operational and physical parameters of the rotor system. In this section, the theory and test data of Phase I are used to evaluate the amount of noise reduction that can be achieved through the proper choice of rotor system design parameters. The formulas are valid for the conventional square-tipped blade with uniform inflow.

The work in Phase I has pointed out the importance of tip speed and aerodynamic conditions at the tip in noise generation. The intensity of the tip vortex and unstable flow near the tip also affect rotor aerodynamic efficiency. A company-sponsored research program to improve rotor efficiency by modification of the tip planform achieved increases in efficiency and reductions in noise. Reduction of tip vortex induced velocity, by approximating an elliptical load distribution, was effective in reducing noise.

Effect of Blade Area, Tip Speed and Lift Coefficient

The theoretical and experimental results of Phase I have shown that the most important parameters governing noise generation are blade area, tip speed and lift coefficient (or angle of attack). The relationship can be formalized as follows:

$$I = \frac{\rho V}{\rho c} K (V_T)^6 A_B (C_L)^2 \qquad (27)$$

The parameters V_T, C_L, and A_B also govern the thrust of the rotor system, as can be seen from the following basic relationship:

$$T = \frac{1}{2} \rho V^2 C_L A_B \qquad (28)$$

Although the above equation assumes a two-dimensional section with velocity V for the purpose of noise estimation, we can let the velocity V be that at the 0.7 radius and assume that C_L is the lift coefficient at a mean angle of attack.

Since the same three basic parameters appear in the equations for noise generation and lift, trade-offs between these parameters for noise control will directly affect lift. However, the appearance of blade

22

velocity, V, to the sixth power in the noise equation allows for limited reduction of tip speed without sacrificing lift.

In Figure 28, calculated overall vortex noise levels are shown for a range of tip speeds with corresponding blade areas to maintain lift. The curves shown are for coefficients of lift of 0.4 and 0.2. These curves are for thrust of 20,000 pounds. The effect on vehicle weight of the changes in blade areas necessary for practical rotor system designs was not considered.

The curves show that sharp decreases in overall vortex noise can be achieved by reduction of the tip Mach number. However, as mentioned above, the larger and heavier blade systems have to produce more thrust to maintain the same payload. The noise associated with the increased thrust partially offsets the reduction shown in Figure 28.

The effect of thrust on the overall vortex noise is shown in Figures 29 and 30. The slope of the curves is approximately 20 times the log of the thrust ratio. Because of the wider variation in tip speeds, the CH-53A system curves show more clearly that tip speed is more important than angle of attack in reducing the vortex noise. For equal thrusts and blade area, reducing the tip speed necessitates increasing the angle of attack. However, the reduction in noise level due to lowering tip speed from 800 to 630 feet per second is about 5 db, even with this compensating increase in angle of attack.

Similar curves can be constructed for any desired thrust by using the vortex noise equation developed in Phase I (equation 6). Selection of rotor design parameters can be made with respect to noise and reconciled with other mission requirements.

Elliptical Tip Loading

Although a limited amount of vortex noise reduction can be achieved by trade-offs between tip speed, blade area and thrust coefficient, a more fruitful area of noise reduction was discovered during tests of blades having elliptical blade loading at the tip. Figure 31 shows the planform for a trapezoidal tip and the standard square-tipped blades studied in the remainder of this report. The trapezoidal shape was adopted as an approximation of the elliptical blade loading. It was expected that elliptical loading would reduce the induced velocity of the tip vortex and thereby increase lifting efficiency.

At the onset of the program it was anticipated that some noise reduction would result. The noise reduction proved to be substantial and appeared to be directly related to increased efficiency.

23

In Figure 32, the overall vortex level is plotted against load for three tip speeds. The tip speeds are the same as those in Figure 29. Except for the tip change, the rotor system is identical to that plotted in Figure 29. The reference line from Figure 29 is repeated to allow direct comparison of the levels. It is interesting to note that the greatest difference between the square and elliptical tip noise levels is at low thrust. The sound pressure levels of the elliptical tips increase more rapidly with increased thrust. At high thrust the difference between the two designs is much smaller. At the normal disk loading of about 19,000 pounds for this size rotor, the reduction in overall noise is about 7 db.

Figure 33 shows the spectra for both square and trapezoidal tip blades at the extremes of the usual range of angles of attack. The spectra for the trapezoidal tips show much less noise in the octave containing the Strouhal frequencies. Each of the elliptical spectra showed a rise in the last octave which is unexplained. The square-tipped blade in Figure 33 is evidently experiencing stall, as discussed in Phase I, because of the secondary peak in the 1200 to 2400 octave. For the same pitch angle the trapezoidal tip still appears to be below the onset of stall.

Figure 34 shows the relative levels of the 300 to 600 octave which contains the Strouhal frequencies over a range of loads. The reduction in the vortex noise at the Strouhal frequencies is obvious. Also it can be seen that above 19,000 pounds the noise in this key octave increases more rapidly with load for the trapezoidal tip.

The reduction in tip vortex strength deduced from the reduction of Strouhal frequency noise is also demonstrated by less modulation of the noise amplitude as shown in Table VIII. Modulation, which results from movement of the source relative to the point of observation, depends on the strength of the moving source. If the moving source is much stronger than the average over the field, the modulation is greater.

Recommendations

Main rotor vortex noise can be reduced by reducing rotor tip speed and by improving load distribution at the tip. It is recommended that minimum tip speed consistent with good aerodynamic design be used. In addition, reduction of the induced velocity of the tip vortex (core thickening) will result in substantial vortex noise reduction without loss in efficiency. Vortex noise reductions of from 7 to 10 db have been achieved with this approach. Since vortex noise falls in a frequency range for which hearing acuity is high, it can be important in determining detectability, as can be seen in Figure 35. The tactical potential of good blade tip design is therefore apparent.

24

ROTATIONAL NOISE REDUCTION

Reduction of Noise Due to Steady Blade Loadings

Far field rotational noise due to steady blade loading and its relation-
ship to the physical parameters of propeller systems are described
mathematically by Gutin (Reference 11). This relationship has been put
into graphic and tabular form (References 3, 15,and 16) which, in
combination with aerodynamic and weight considerations, makes the
matter of parameter selection for low noise straightforward. Additional
investigations (References 12, 13,and 27) have defined the trade-offs
necessary to obtain lower noise levels. These studies, in many cases,
have concentrated on the propeller noise as it affects aircraft detect-
ability. Aircraft detectability relates noise generated by an aircraft to
the ability of a human to detect its presence audibly. Detectability is
extremely important in military applications, as an aircraft's acoustic
detectability is a factor in determining combat effectiveness and proba-
bility of survival. The concept of detectability will be used as a basis
for evaluation of rotor noise alleviation techniques.

Figure 35 from Reference 20 shows the minimum detectable level
of aircraft noise in a low noise background. The level up to approxi-
mately 250 cps is the threshold of hearing (Reference 6). Compare this
with an S-58 helicopter noise spectrum shown in Figure 36. It is
obvious that the fundamental (normally between 15 and 20 cps) of the
main rotor blade passage noise would have to be at a much higher level
than the higher harmonics in order to determine detectability. In
general, the fundamental component of rotor rotational noise is below
audible level and is not heard. Instead, blade passage harmonics and
modulated vortex frequency noise are heard and incorrectly identified as
blade passage frequency noise. It is recognized then that the fundamental
of rotational noise of helicopter rotor systems is not important in deter-
mining detectability. While Gutin theory does not accurately predict the
level of the harmonics, it is adequate for estimating the relative effect
of design parameters.

Reduction of Noise from Nonuniform Rotor Loading

This study is based on the assumption that first harmonic rotational
noise is not significant in judging loudness, and that harmonic levels
resulting from steady inflow to the rotor will vary directly as the funda-
mental for which noise control methods are already known. To mini-
mize the acoustic signature of a helicopter, techniques must be developed
to reduce the harmonic content of rotational noise.

According to Gutin, the noise level of the individual harmonics decreases rapidly with harmonic number, as shown in curve A of Figure 37. Gutin's equation assumes that all blade loading is concentrated at a single point on the blade. This loading is simulated in curve A. When the concentrated loading is spread out over a larger segment of the blade, the upper harmonics increase in level. This implies that concentration of blade loading over a smaller disk area, which might be accomplished by reducing the diameter, for example, results in lower harmonic noise levels. This relationship cannot be utilized, however, because the harmonic dropoff gained by concentrating the load would be more than offset by the increase in overall noise level from the higher blade loading.

The fact that redistribution of steady blade loadings cannot be utilized to reduce harmonic noise levels leaves nonuniform loading as the controlling factor in determining harmonic level.

The influence of steady plus 4-per-rev blade loading on harmonic noise levels is shown in Figure 38. Three different levels of 4-per-rev plus steady loading were used to calculate the harmonic noise levels for the S-58 rotor system. The levels were calculated by the methods of Phase II. The rotor system parameters and loads for this hypothetical system are presented in Appendix IX. The harmonic dropoff is substantially affected by the addition of the variable blade loading. For example, the second noise harmonic is now higher than the fundamental and all the levels of the harmonics are increased over those generated by the steady loading.

The 4-per-rev loading contributes more to the level of the higher harmonics than the fundamental does. Calculations were made to determine whether a pattern exists which describes relationship between blade loading and rotational noise levels. The results are shown in Figures 39 to 45, which represent the same information as Figure 38 except that the noise due to steady loading has been removed to show only the result of harmonic loading. The increase in sound pressure level caused by doubling the harmonic loading (from 1/4 to 1/2 of the steady loading amplitude) is not always the 6 db which would result from interaction between the harmonic and the steady loadings. The shapes of the curves change considerably between one blade loading harmonic and the next. The higher blade loading harmonics have a greater effect on the higher noise harmonics and less effect on the lower noise harmonics. Notice that as the blade loading harmonic increases, the noise produced by a given level of loading greatly increases. In other words, the efficiency of conversion from blade loading to noise increases with blade loading harmonic. This effect is shown for blade loadings up to 10-per-rev in Figures 46 and 47, where noise level is plotted against

26

rotational noise harmonic for several harmonic blade loading conditions. This is done for a harmonic loading level of one-quarter the amplitude of the steady component plus the steady loading, but with the noise attributed to the steady load omitted.

To get a better idea of how the noise producing efficiency of blade loading varies with noise and loading, the data of Figures 46 and 47 is cross plotted in Figure 48. The fact that certain blade loading harmonics generate noise most efficiently at certain noise harmonic frequencies is clearly shown here. Again the harmonic blade loading level used here is 1/4 that of the steady loading and the noise attributed to the steady loading itself has been removed. Even when the noise levels due to the steady loading are added to those of Figure 48, as shown in Figure 49, it is quite easy to produce a spectrum where many harmonic levels are higher than the fundamental. The acoustical efficiency of the many blade loading harmonics is the cause of the high levels of rotor and propeller noise harmonics.

If a helicopter is being designed for low detectability, it is essential to control the harmonics of blade loading. The more uniform the inflow, the lower are the blade loading harmonics. Although rotor system dynamics and aeroelastic characteristics play a role in determining the inflow pattern, the most important acoustic consideration is the presence or absence of wake interaction from other blades or rotor systems.

Quantitative analysis of the pressure field generated by a rotor and its blade loading is difficult. Improved correlation between measured and predicted blade loading has been obtained by replacing steady aerodynamic inflow theory with variable induced inflow theory (References 8 and 31). Further work is required, however, to generate harmonics of higher order analytically with any degree of accuracy. Figures 39 to 45 show the importance of the higher order blade loading harmonics in determining harmonics of rotational noise. As an example, Figure 46 shows that if a 2-per-rev blade loading, of 1/4 the amplitude of the steady, were present in addition to the steady, the fourth harmonic of rotational noise would be increased by 7 db. If there were a 5-per-rev blade loading of 1/4 the magnitude of the steady in addition to the 2-per-rev and steady loadings, the level of the fourth harmonic of rotational noise would be further increased by 41 db. For a rotor with n number of blades, it appears as though the mth harmonic of rotor noise is most sensitive to the $m(n-1)$ loading harmonic. To determine higher order noise harmonics accurately, it appears as though there is a need for loading data of much higher harmonic content than presently is available from measurements or analysis.

27

Design Recommendation

It is concluded from the Phase III study that it is necessary to control rotor harmonic loading in order to control rotational noise. Means are not presently available, however, to predict the nonuniform portion of rotor loading to the accuracy required for use in the rotor noise program. Gutin's theory of Reference 11 is adequate to predict trends only for first harmonic rotational noise under steady inflow conditions. The charts of References 3, 15, and 16 then become useful in determining the acoustic effect of blade parameter changes, but not the absolute level. For predicting rotational noise, for even relatively uniform inflow conditions, the analysis presented in Phase II should be used. The required input data for such predictions must include up to at least the m times n harmonic of blade loading. Here n is the number of blades and m is the desired harmonic of rotational noise. Since the state of the art does not allow prediction of higher than the fourth or fifth harmonic of blade loading, little can be concluded as to the parametric effects of design changes on harmonics of rotational noise.

In addition to the general requirements of low tip speed and blade loading, it is recommended that the blade tip be designed so that loading is distributed as evenly as possible and local turbulence is held to a minimum. This is the same requirement as that specified for vortex noise control and can be accomplished with tips such as the trapezoidal variety.

BLADE SLAP

Discussion

Blade slap is the sharp popping sound produced by a helicopter rotor during certain flight conditions. This characteristic was extensively investigated in this study to define the mechanism of blade slap and means of controlling it.

Results of this study and that described in Reference 2 indicated that blade slap consists of high-amplitude rotational noise plus highly modulated vortex frequency noise. The slapping or popping noise occurs when the blade has rotated approximately 270 degrees from the tail during forward flight. Reference 5 indicates that blade slap is due to amplitude modulation of broad-band noise during stall. It can be seen in Figure 33 and in Figure 2 of Reference 33 that vortex noise levels are a minimum of 7 db higher for the stalled (separated flow) condition than for the unstalled condition.

28

Figure 14. Single Rotor Helicopter
Typical Angle of Attack Distribu-
tion

The contention that blade slap
is associated with blade stall can be
demonstrated as follows. Figure 14
shows the angles of attack around
the disk of a single rotor helicopter
during 100-knot forward flight. The
maximum angle of attack occurs at
an azimuth angle between 270 degrees
and 360 degrees. As speed is in-
creased, the angle of attack in this
area is increased. Ultimately, stall
will occur at the tip and will spread
toward the rotor hub. The occur-
rences of stall and angle of attack
change are explained quite clearly in
Reference 9. These variations in
angle of attack are typical for a
single rotor helicopter. Experi-
mental data from Reference 10 on a
rotor system experiencing stall
(Figure 15) shows that calculated
results (dotted line) are reasonably accurate and that the region around
270 degrees is indeed the area which is most susceptible to stall during
high speed flight. Since both blade slap and stall occur near the 270
degrees azimuth position, it can be concluded that slap is related to
blade stall for this flight condition.

Pilot reports state that the blade slap occurs with high blade loading
such as that encountered in high speed forward flight or in a heavily
laden condition. They also report slap when making powered descent
and in transition to autorotation. Where stall is imminent, a perturba-
tion in the aerodynamic inflow, such as the downwash of another rotor
or an encounter with a shed vortex from a preceding blade, may be
sufficient to induce the stall.

FORWARD

MEAS RED
STALL AREA

40 MPH
M_T=0.36 CALCULATED
STALL AREA

70 MPH
M_T=0.4

70 MPH
M_T=0.36
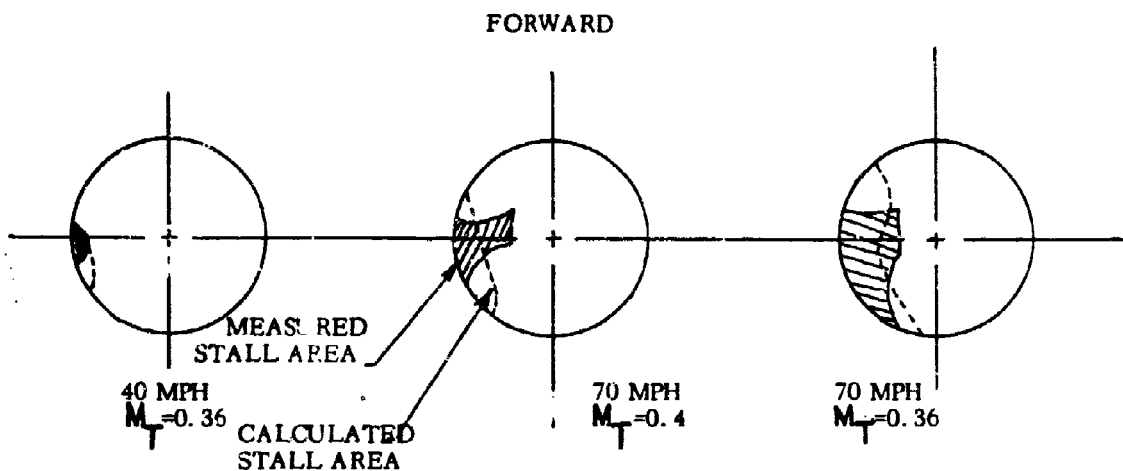
Figure 15. Occurrence of Stall in the Rotor Disk

With tandem rotor helicopters, the lower rotor encounters the downward induced flow along with shed vortices in a portion of its disk area. The intersection of these vortices and the resulting sudden change in angle of attack and flow separation cause nearly continuous slapping. A comparison of the levels of a single rotor (S-61) helicopter and a tandem rotor (V-107) helicopter during approach to landing is shown in Figure 16. The ships are of approximately 18,000-pound design gross weight and are performing the same maneuver. During the maneuver, both aircraft are producing impulse type noise.

30

120

SPL - db(reference 0.0002 dyne/sq. cm.)

110

100

90

80

70

63 125 250 500 1000 2000 4000 8000

△ TANDEM ROTOR
□ SINGLE ROTOR

OCTAVE BAND CENTER FREQUENCIES
IN CYCLES PER SECOND
DISTANCE 70 FEET FROM BOTH SHIPS
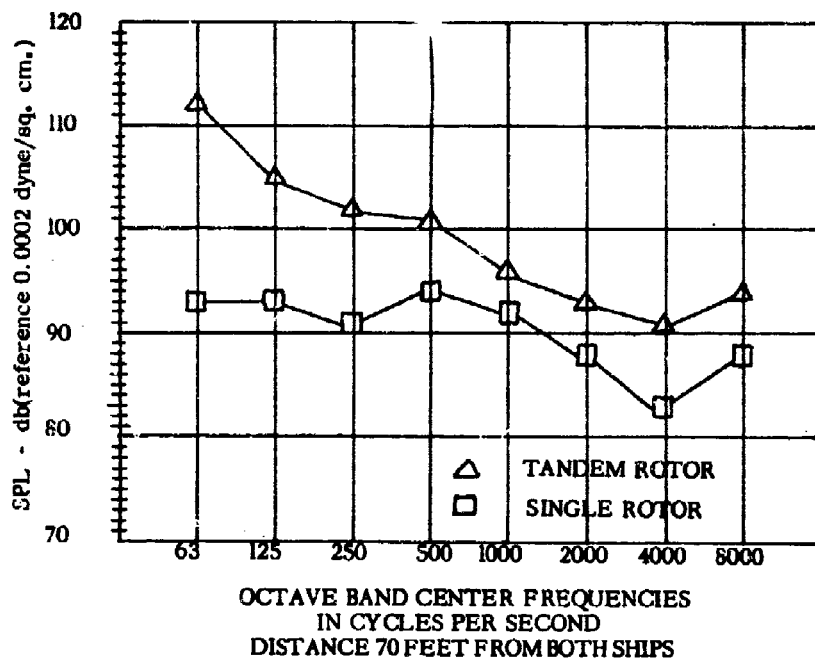
Figure 16. Single versus Tandem Rotor Noise in Approach
(Reference 34)

The frequency content of the noise for the two helicopters is similar.
The considerably higher noise in the 20-to 75-cps octave indicates that
the tandem helicopter experiences corresponding changes in lift in the
overlap region. As was shown in Phase II, the periodic change in lift or
blade pressure causes high level noise at the blade passage frequency
and its harmonics. Although momentary tip stall may occur on the
single rotor ship, the fluctuation in lift is less intense. Consequently,
it generates little more noise than in the unstalled condition.

Tests of blades with square and trapezoidal tips were made by
Sikorsky Aircraft. The trapezoidal tips are designed to reduce the
induced velocity of the tip vortex from that of the square-tipped blade.
This lessens the depth of vortex noise modulation and also leaves less
of a disturbance in the flow field to interact with the other blades. The
differences between noise spectra of the two blade types are shown for
various power and speed conditions in Figures 33 and 34. Details of
the test are explained in Phase I.

31

The phenomenon of compressible drag divergence, which occurs with stall, is also related to blade slap. When drag divergence occurs, drag increases and power is consumed. The increase in drag is due to the unstable formation of local shock waves which transform energy into heat and pressure pulses. If sufficiently strong, these shock waves contribute to the blade slap noise.

The Phase II calculation procedure is completely general, and as such will predict the harmonic content of any condition, including blade slap. Blade slap was not detected during the measurement program. In order to determine whether blade slap could be predicted by the Phase II analysis, it was, therefore, necessary to simulate a blade loading condition which would induce blade slap. Since blade slap occurs during blade stall, blade pressure data recorded during the occurrence of blade stall was used as a basis for the harmonic loading input. Blade pressure time histories at 85 percent span for the 80-knot 1/2 g turn are shown in Figure 17. From analysis of the pressure time history at the trailing edge, it was evident that stall was present. This trace was analyzed for harmonic content over one blade revolution. The resulting harmonics were used as blade loading for the entire chord at the 85 percent span of the rotor system and the noise harmonics were calculated. Noise levels were also calculated using only the steady component of the blade loading. The resulting harmonic distributions are shown in Figure 18 along with the harmonic distribution resulting from steady 80-knot flight on the same S-58. The steady loading spectrum exhibits the usual rapid dropoff in harmonic noise level associated with steady loads alone. The 80-knot cruise spectrum levels drop off also, although not so rapidly. Finally, the spectrum generated using the impulsive airloads experienced during blade stall shows extremely high harmonics.

Figure 17. S-58 Blade Differential Pressure Time History During An 80-Knot, 1/2 g Turn at 85 Percent Span - A Condition of Partial Blade Stall

32
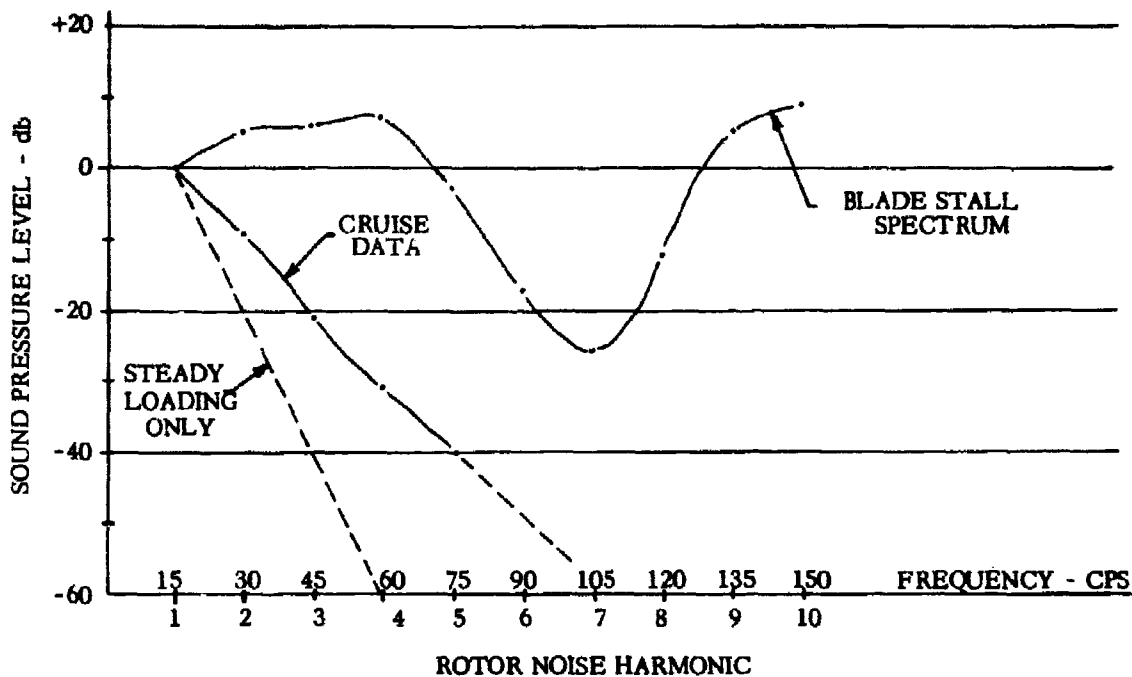
Figure 18. Rotational Noise Harmonic Content

This spectrum is similar in shape to the blade slap spectrum measured
on an SH-3A helicopter during an abnormally rough flare from level
flight to hover, at which time the blades were experiencing localized
blade stall. Although the spectrum shown is limited to 150 cps, blade
slap extends over a frequency range of 20 to over 1000 cps, and
increases vortex noise levels as well as the rotational noise harmonic
levels. Reference 1 also substantiates this point. Thus, if detailed
blade surface pressures are available, the blade slap rotational har-
monic spectrum can be predicted. As shown in Figure 17, stall can
be a localized phenomenon, requiring detailed blade surface pressures
to be described adequately. These prediction methods, however, are
not presently available. It appears that the best basis upon which to
judge the likelihood of blade slap occurrence is aerodynamic stall
criteria.

Design Recommendations

For minimal rotational noise and blade slap, the obvious design
guidelines are to use the lowest possible tip speed and to use shaped,
twisted blades which distribute tip loading and substitute sheet vortices

for the stronger tip vortices. Although blade stall appears to be the major cause of blade slap, compressible drag divergence, i.e., Mach effects, cannot be ignored. When blade elements are in stall, compressible drag divergence is also present. To make blade design recommendations for reduced blade slap strictly on the basis of reduced stall would be premature at this time, since blade design for reduced tendency to stall may well increase the extent of drag divergence. Further study is therefore needed to define the relationships between blade slap and the degree of stall, drag divergence, and tip vortex induced velocity if positive blade design recommendations are to be made.

TABLE I

CALCULATED VORTEX NOISE FREQUENCIES AND THEIR RELATIVE
INTENSITY FOR THE CH-53A ROTOR BLADE AT 30,000 POUNDS THRUST

r/R	α (degrees)	M	V (ft. sec)	h' (ft)	f^* (cps)	Down From Tip Level (db-db at Tip)
0.300	3.31	0.187	209	0.367	154	-31.3
0.450	3.54	0.280	313	0.375	225	-20.9
0.600	3.44	0.374	418	0.371	300	-13.3
0.700	3.30	0.436	487	0.366	360	- 9.3
0.750	3.20	0.467	522	0.362	390	- 7.5
0.800	3.10	0.499	556	0.359	420	- 5.9
0.850	3.00	0.530	591	0.355	450	- 4.3
0.900	2.84	0.561	626	0.349	480	- 2.8
0.950	2.64	0.592	661	0.341	520	- 1.3
0.975	2.45	0.608	679	0.334	550	- 0.7
1.000	0.00	0.624	696	0.000	-	0.0

$$* \quad f = \frac{S_t V}{h'}$$

where $S_t = 0.28$

TABLE II
OVERALL VORTEX NOISE LEVELS

Rotor Speed (rpm)	Thrust (pounds)	SPL Calculated by Equation 6 (db*)	SPL Measured (db*)	SPL Calculated by Equation 5 (db*)
		CH-3C ROTOR SYSTEM		
183.0	13,400	78	76	79
	16,200	80	79	
	18,700	81	81	
	20,500	82	82	
203.0	16,300	82	81	82
	18,100	83	81	
	19,900	83	82	
	21,400	83	83	
213.0	14,500	81	81	83
	18,200	83	83	
	20,000	83	83	
		CH-53A ROTOR SYSTEM		
166.0	24,000	82	80	83
	28,400	83	81	
	32,000	84	83	
	36,200	85	83	
	39,000	86	85	
185.5	25,000	83	83	85
	30,100	85	83	
	36,200	86	85	
	41,600	87	87	
215.0	23,700	84	85	89
	29,600	86	86	
	37,900	88	89	
	43,520	89	90	

* Ref = 0.0002 dyne/sq. cm.

TABLE III

PHYSICAL CHARACTERISTICS OF TEST ROTOR SYSTEMS

	CH-3C	CH-53A
Number of blades	5	6
Diameter (feet)	62	72
Blade area (ft^2)	217	368
Solidity	0.078	0.115
Disk area (ft^2)	3020	4070
Airfoil	0012	0012 Modified
Chord (feet)	1.50	2.16
Rotor speed (RPM)	183	166.0
	203	185.5
	213	215.0
Tip speed (ft/sec)	595	625
	661	696
	692	810
Tip Mach number	0.532	0.591
	0.586	0.625
	0.613	0.726

TABLE IV
COMPARISON OF FIRST HARMONIC NOISE CALCULATIONS BY GUTIN'S EQUATION AND BY THE SIKORSKY PROGRAM

σ * (degrees)	Sikorsky Sound Pressure (psi)	Sikorsky SPL (db**)	Gutin Sound Pressure (psi)	Gutin SPL (db**)
-45	1.6×10^{-5}	74.8	1.58×10^{-5}	74.7
-30	2.92×10^{-5}	80.0	2.82×10^{-5}	79.8
-15	3.41×10^{-5}	81.4	3.29×10^{-5}	81.0
0	2.69×10^{-5}	79.3	2.58×10^{-5}	79.0
15	1.32×10^{5}	73.2	1.24×10^{-6}	72.6
30	3.39×10^{-6}	61.4	1.87×10^{-6}	56.2

* Elevation angle = 0° in rotor plane, positive above, negative below

** Ref = 0.0002 dyne/sq. cm.

TABLE V
FLIGHT TEST PARAMETERS

Test weight-pounds	approximately 12,000
Number of blades	4
Blade radius-feet	28
Blade twist-degrees	-8
Blade chord-feet	1.367
Test rotor speed-rpm	212
Test engine speed-rpm	2400
Test rotor-angular velocity-radians/second	22.2

TABLE VI

MEASURED AND CALCULATED FIRST HARMONIC NOISE LEVELS

Distance (Feet)	Speed (Kts)	Power (hp)	Torque (lb-in)	Thrust (lb)	Gutin Level (db)*	Program Level (db)*	Measured Level (db)*
300	40 (cruise)	651	192760	11761	71.8	91.0	91.0
300	80 (cruise)	647	180469	11769	71.7	89.0	88.0
300	110 (cruise)	1016	296530	11750	72.7	91.8	89.0
300	70 (pullout)	650 **	183000 **	11760 **	71.7	91.0	87.0
600	0 (hover)	1016 **	300000 **	12000 **	66.2	73.8	70.76

* Ref = 0. 0002 dyne/sq. cm.

** Estimated

TABLE VII

BLADE LOADING TABLES USED IN
PROGRAM

Blade Loading Data Table *	Noise Measurement Condition
4	Hover out of ground effect
8	40-Knot cruise
13	80-Knot cruise
19	110-Knot cruise
111	70-Knot cyclic pullout

* Reference 28

TABLE VIII

17-CYCLE-PER-SECOND AMPLITUDE MODULATION: COMPARISON OF CH-3C TRAPEZOIDAL TIP VERSUS SQUARE TIP BLADES

Average Depth of Modulation - db[*]

Octave	Square Tip	Trapezoidal Tip	Difference
150-300	8	5	3
300-600	10	6	4
600-1200	8	8	0
1200-2400	5	4	1
2400-4800	7	4	3
4800-9600	6	4	2
		6	13
		AVERAGE DIFFERENCE	2

[*] DEPTH OF MODULATION $= 20 \log \dfrac{a}{b}$

17 cps
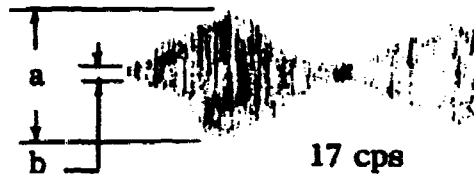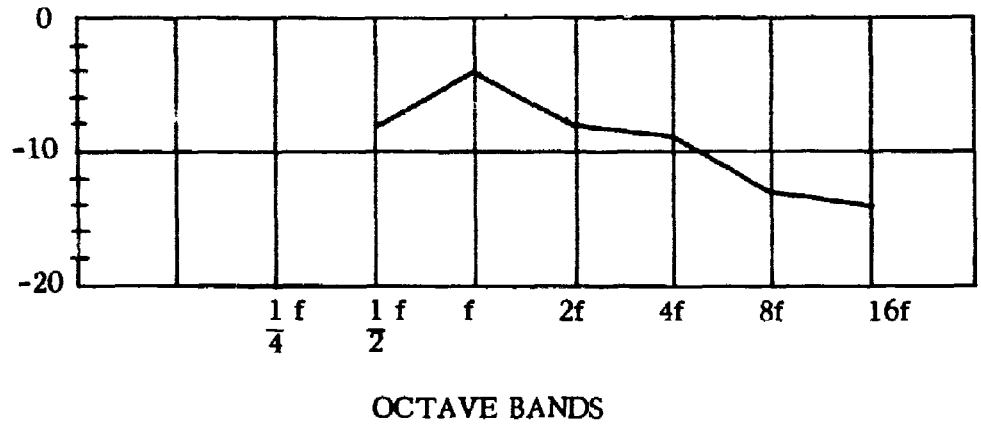
Figure 19.   Spectrum Below Stall
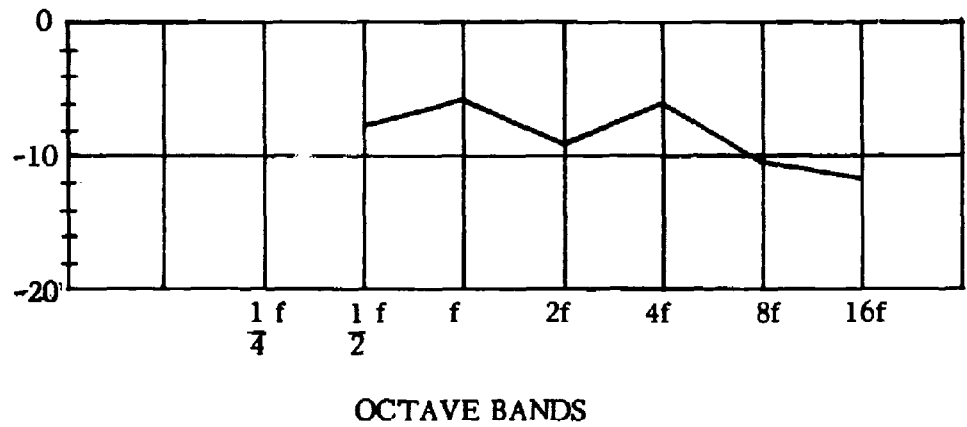
Figure 20.   Spectrum Above Stall
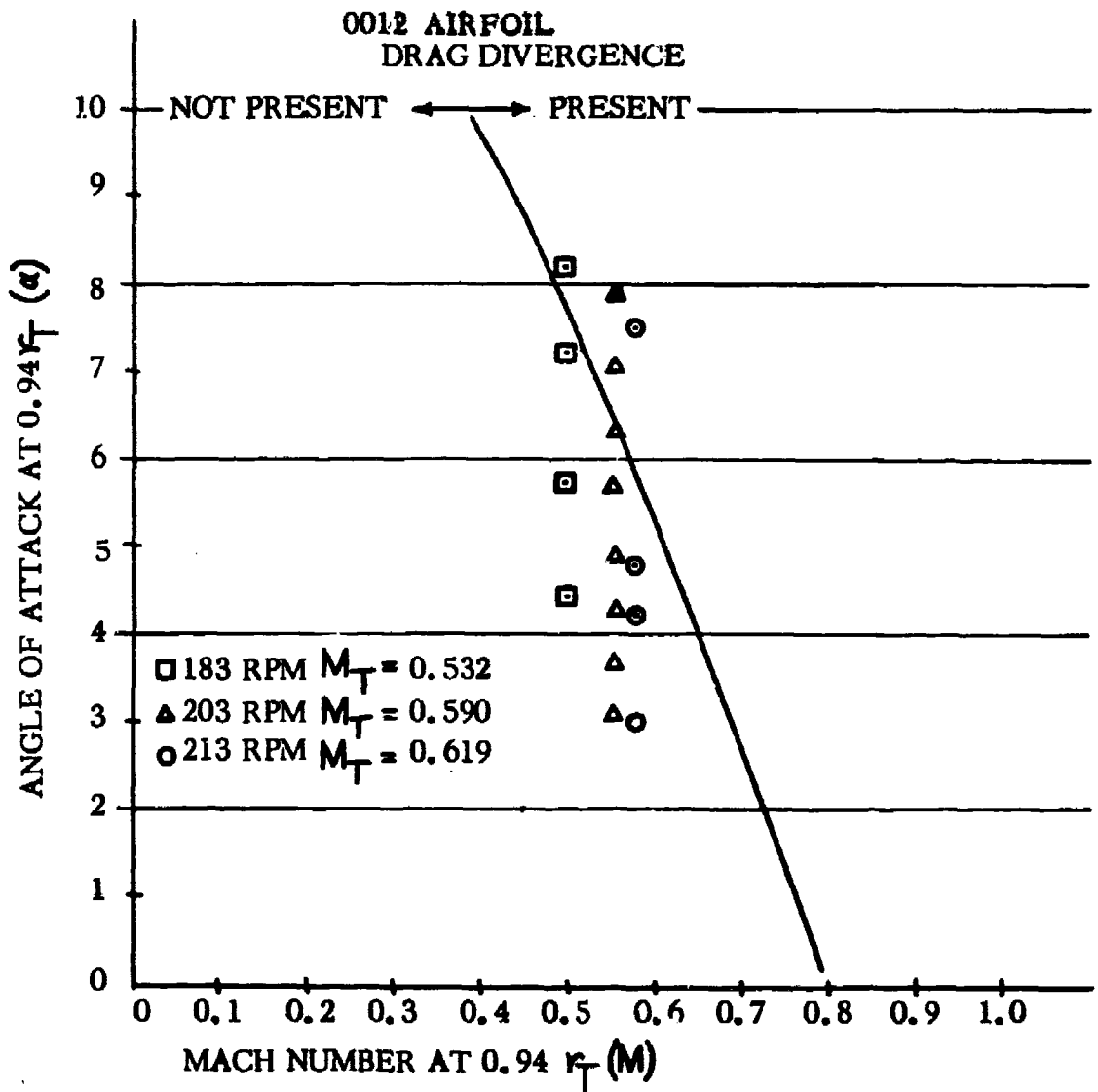
Figure 21. Drag-Divergence Curve for the CH-3C

43
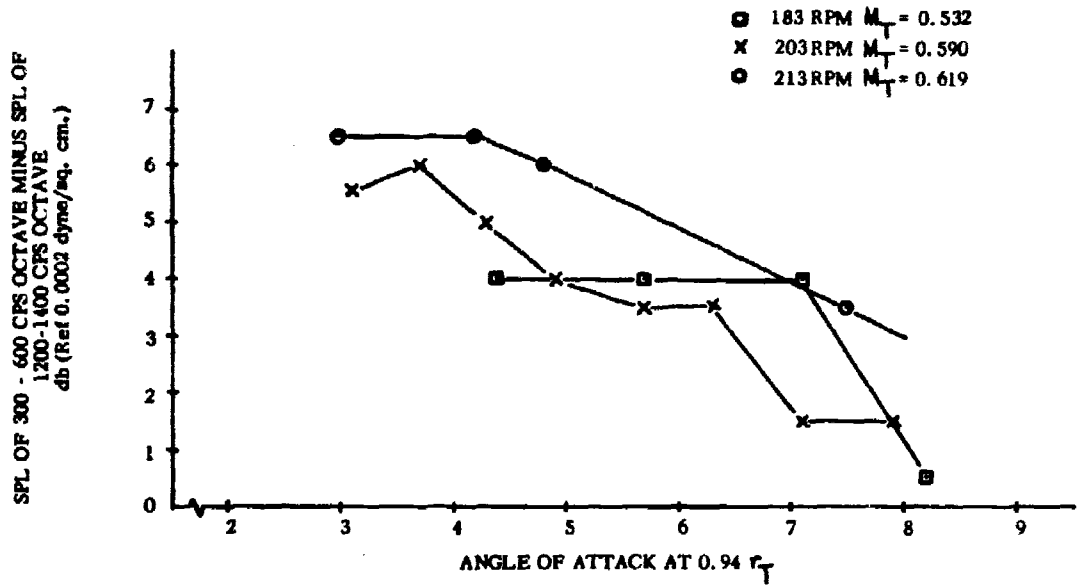
Figure 22. Onset of Drag-Divergence
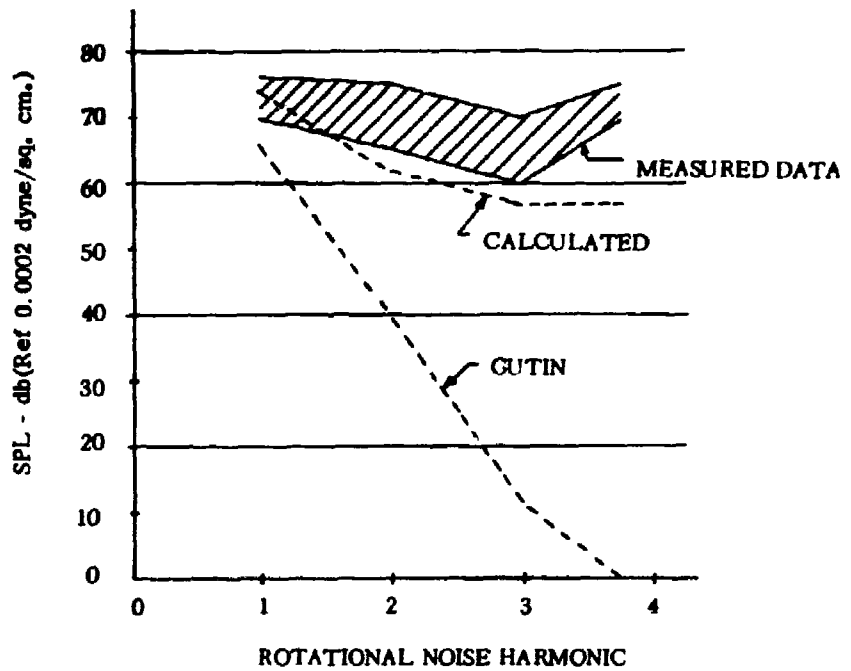
Figure 23. Calculated and Measured Levels - Hover

44
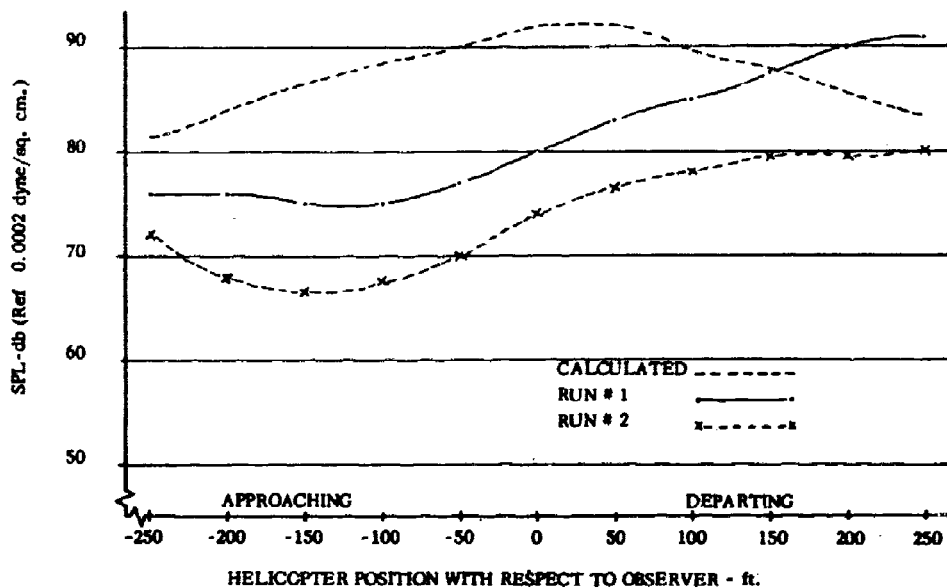
Figure 24 a. Calculated and Measured Levels - 40-Knots - First
Harmonic
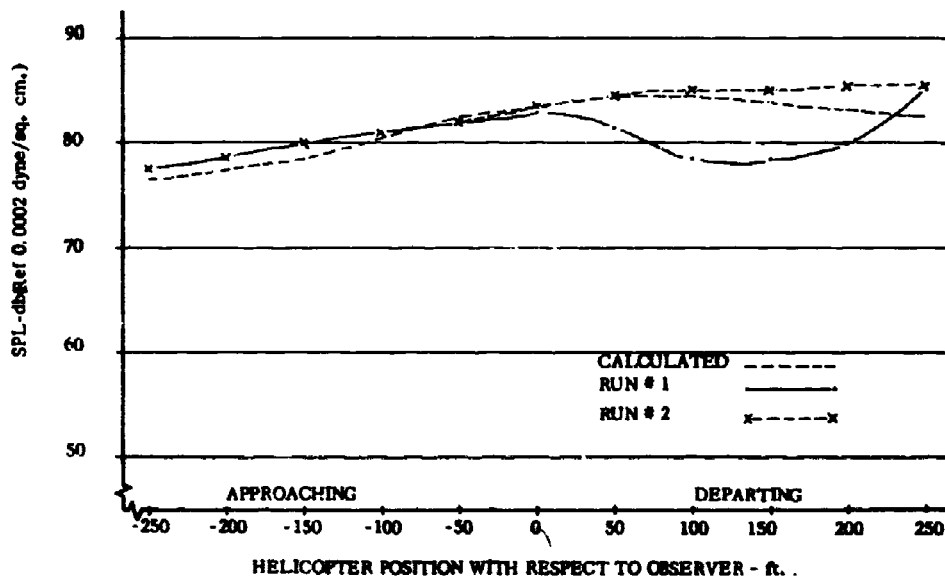
Figure 24 b. Calculated and Measured Levels - 40-Knots - Second
Harmonic

45
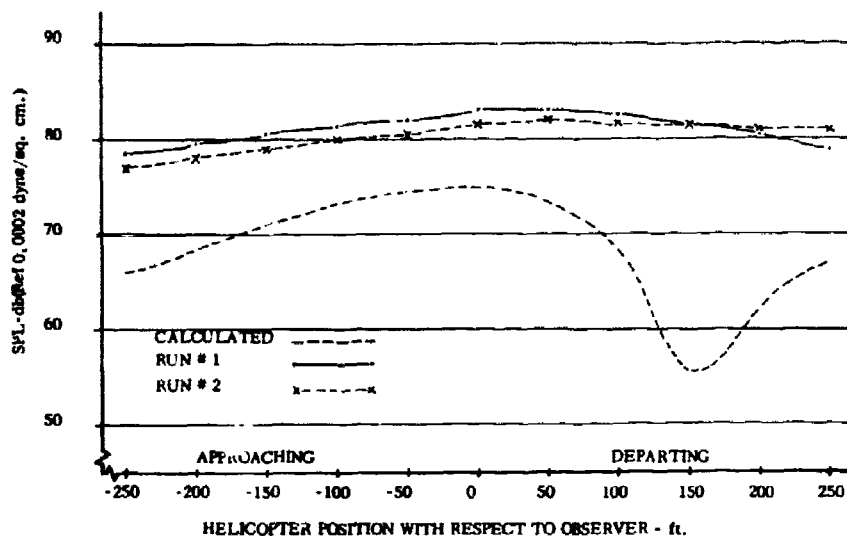
Figure 24 c. Calculated and Measured Levels - 40-Knots - Third
Harmonic
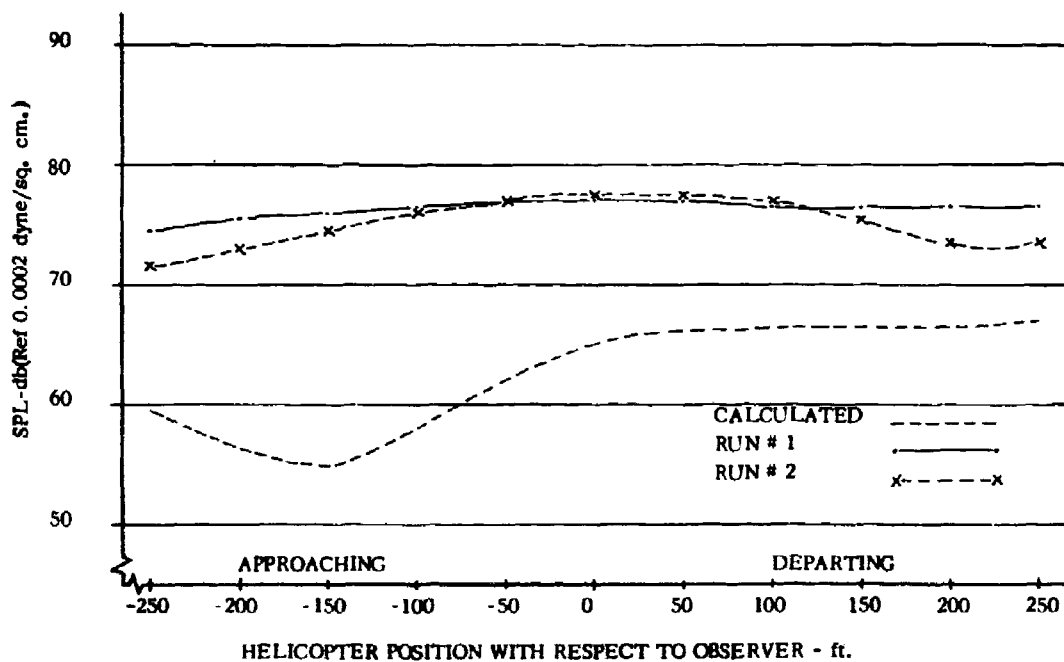
Figure 24 d. Calculated and Measured Levels - 40-Knots - Fourth
Harmonic

46
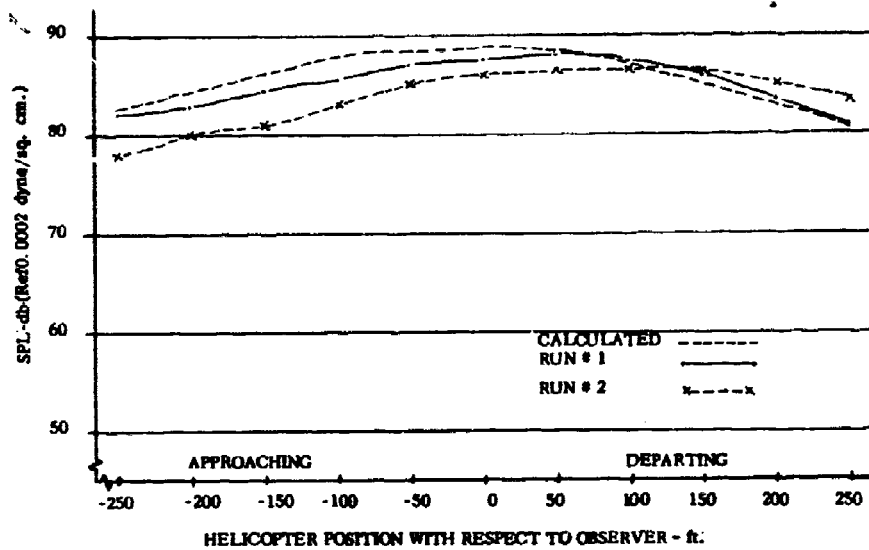
Figure 25 a. Calculated and Measured Levels - 80-Knots - First Harmonic
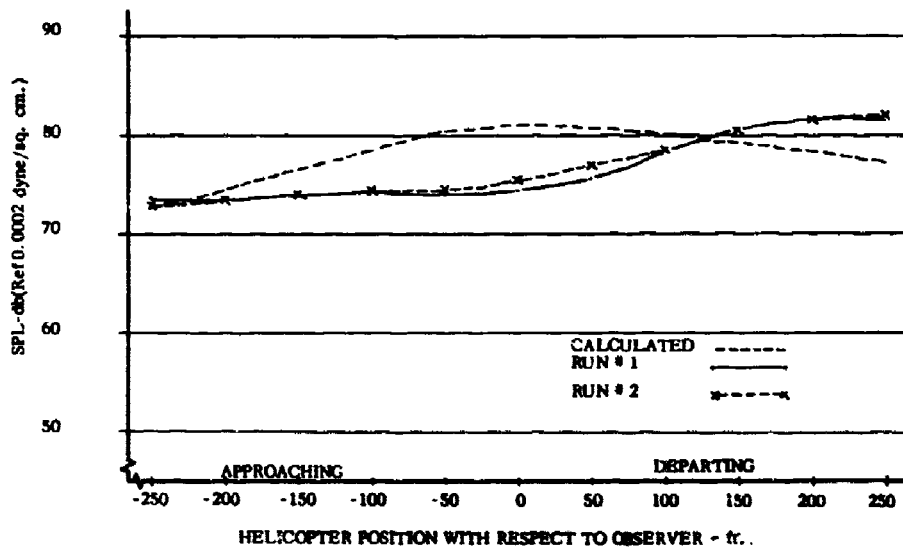
Figure 25 b. Calculated and Measured Levels - 80-Knots - Second Harmonic

47
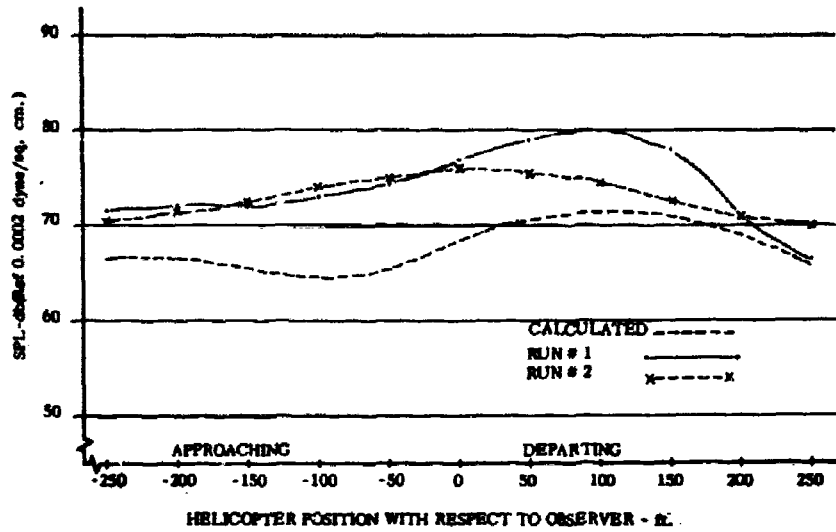
Figure 25 c.   Calculated and Measured Levels - 80-Knots - Third
Harmonic
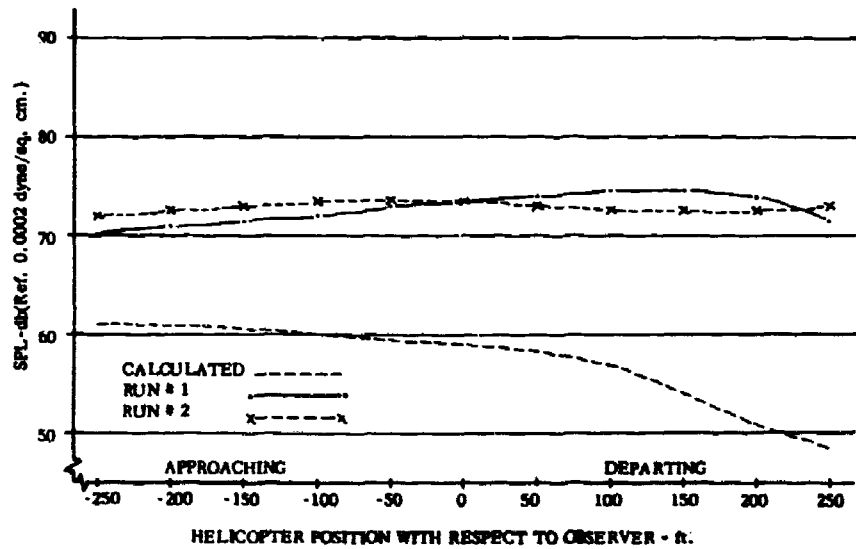
Figure 25 d.   Calculated and Measured Levels - 80-Knots - Fourth
Harmonic

48
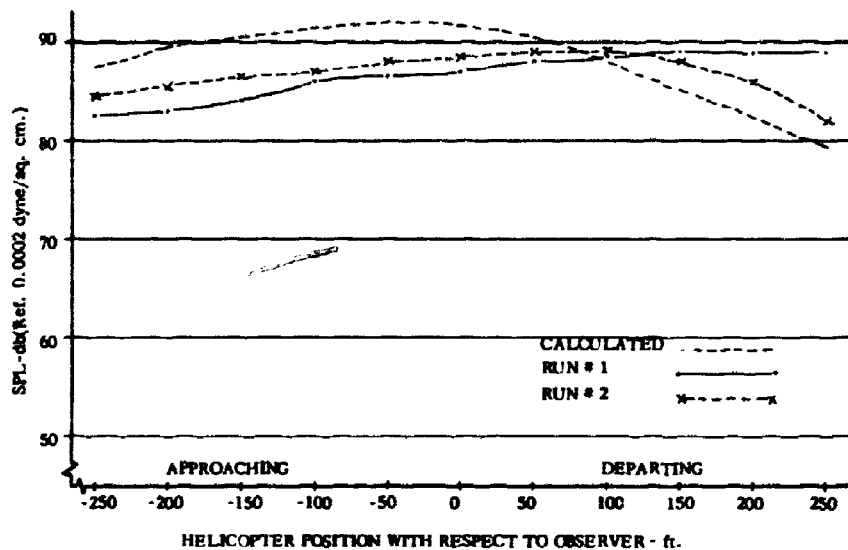
Figure 26 a.   Calculated and Measured Levels - 110-Knots - First Harmonic
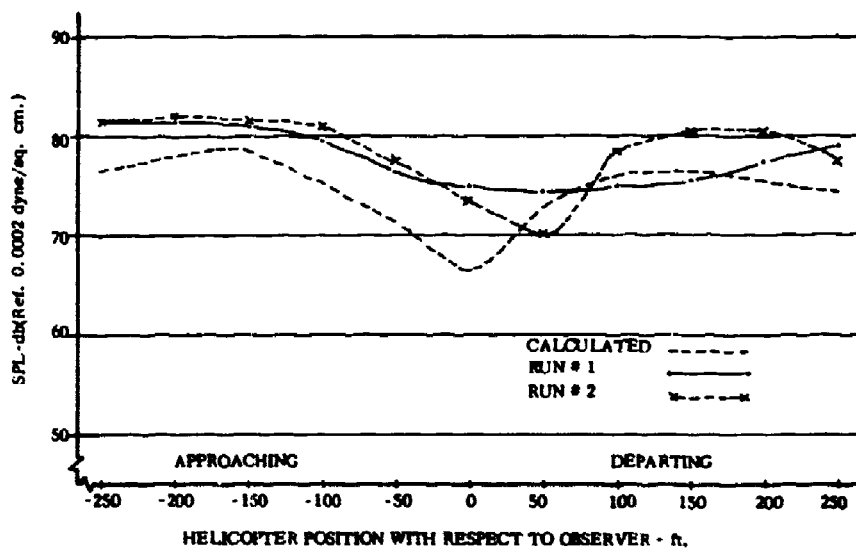
Figure 26 b.   Calculated and Measured Levels - 110-Knots - Second Harmonic
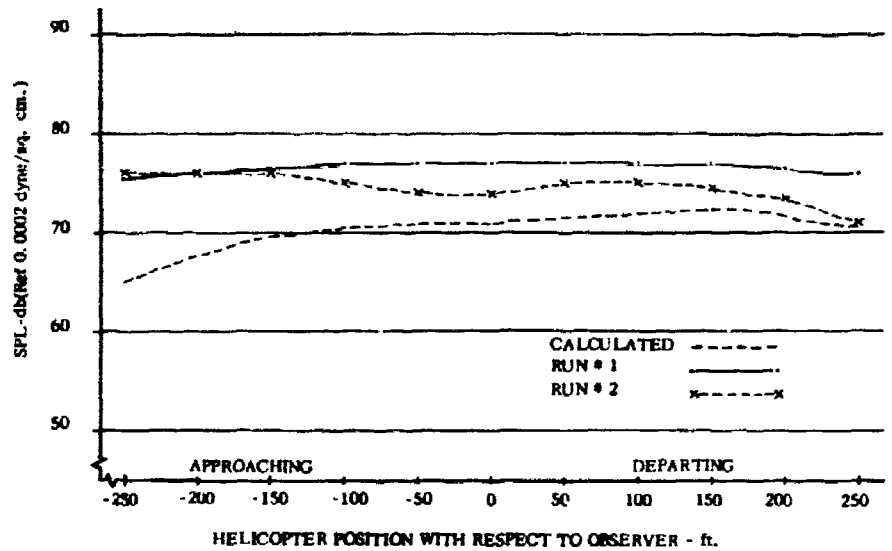
Figure 26 c.   Calculated and Measured Levels - 110-Knots - Third
Harmonic
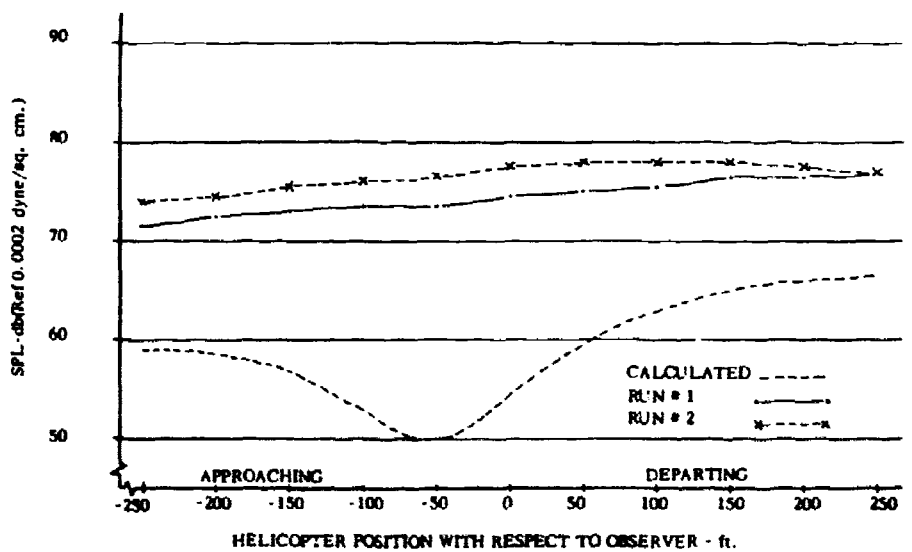
Figure 26 d.   Calculated and Measured Levels - 110-Knots - Fourth
Harmonic
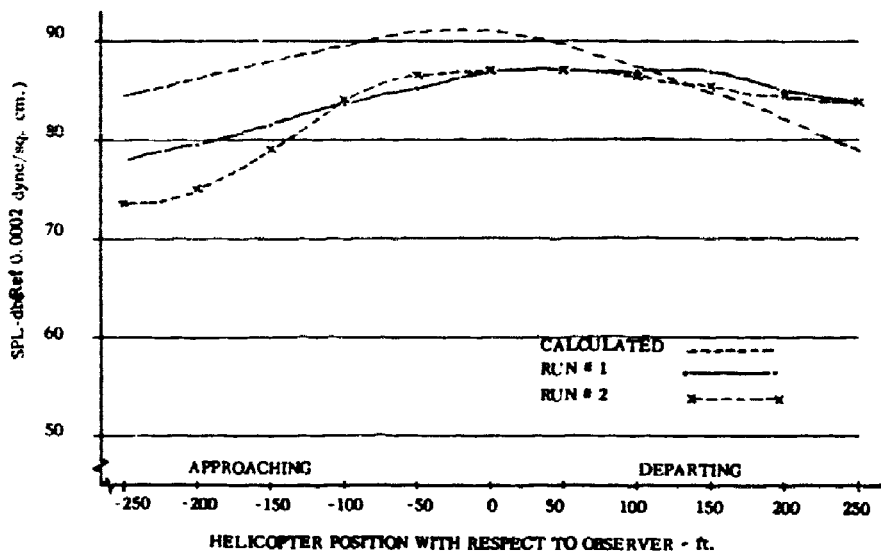
Figure 27a. Calculated and Measured Levels - 70-Knot Cyclic Pullout - First Harmonic
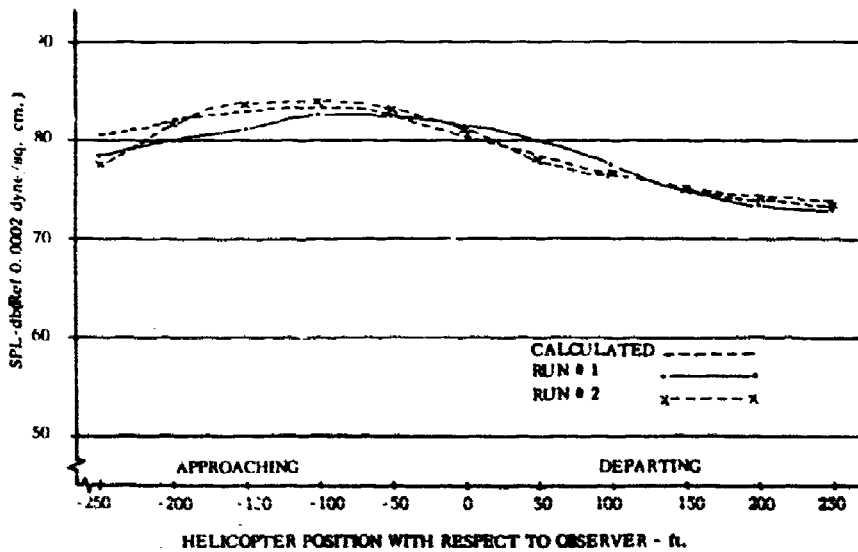
Figure 27b. Calculated and Measured Levels - 70-Knot Cyclic Pullout - Second Harmonic

51
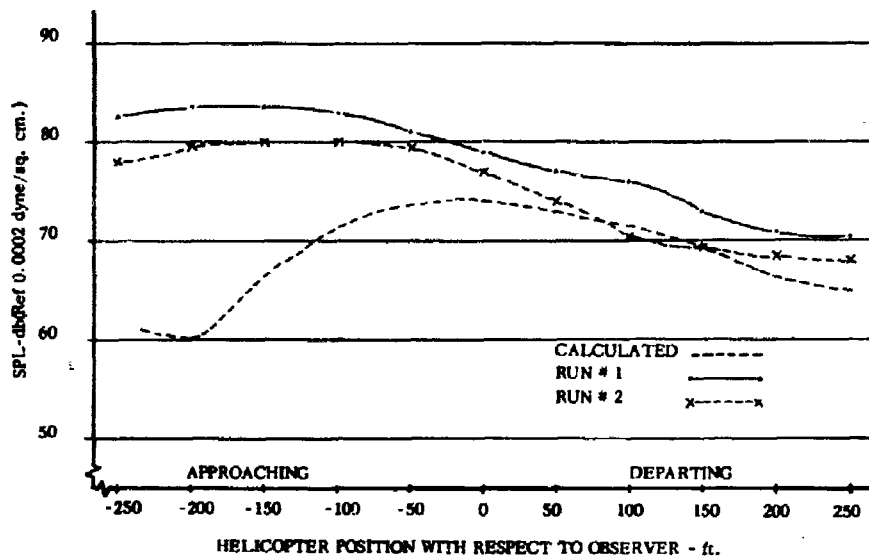
Figure 27c. Calculated and Measured Levels - 70-Knot Cyclic Pullout -
Third Harmonic
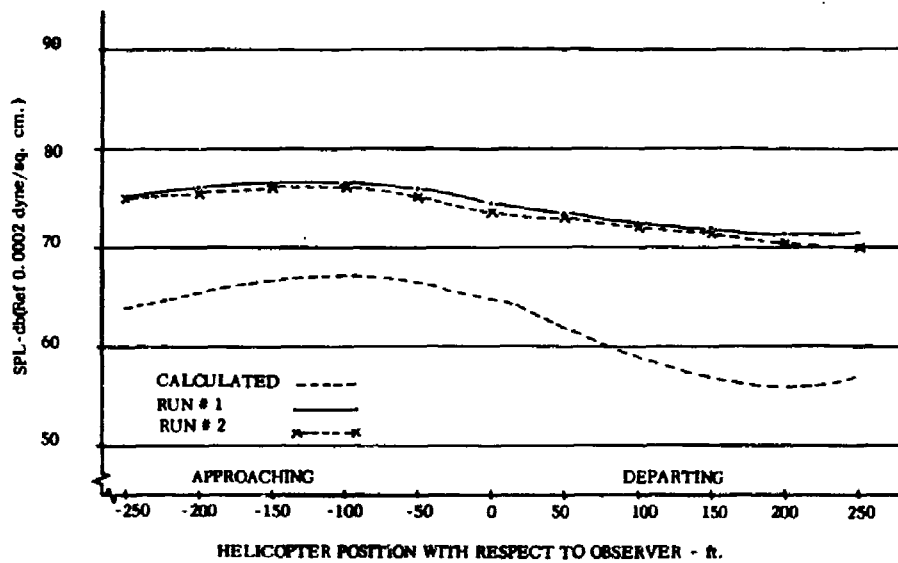
Figure 27d. Calculated and Measured Levels - 70-Knot Cyclic Pullout -
Fourth Harmonic

52
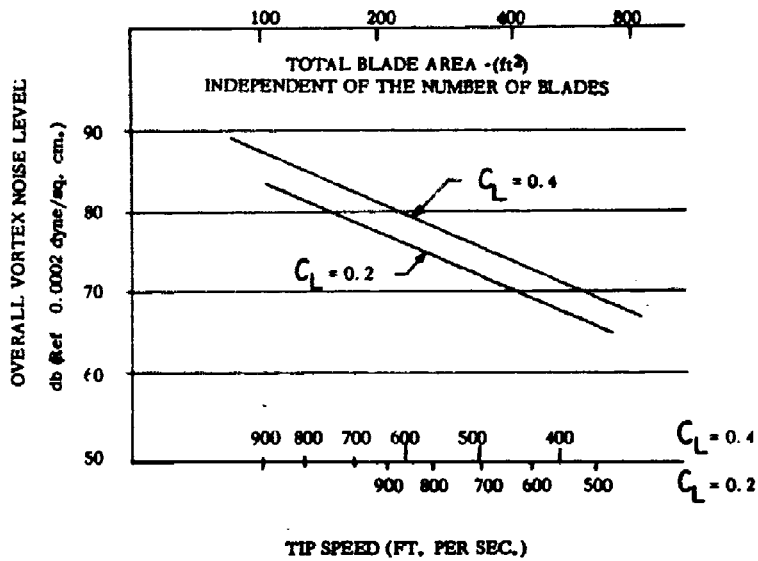
Figure 28. Calculated Noise Levels at 300 Feet, 20,000 Pounds Thrust,
5 Blades

O 183 RPM/591 FPS
△ 203 RPM/661 FPS
X 213 RPM/692 FPS
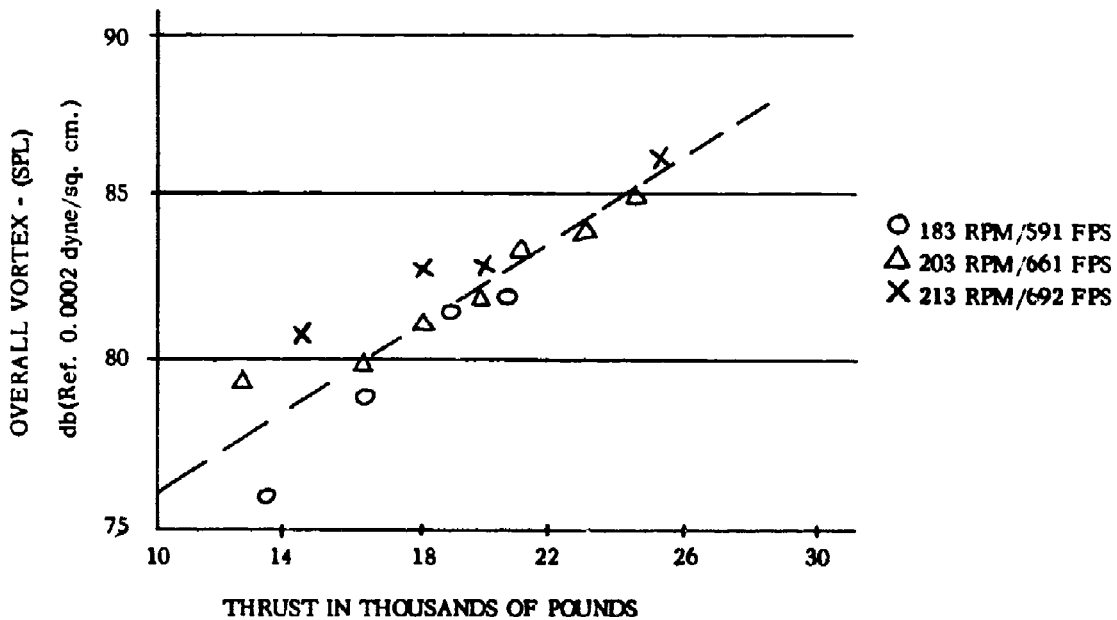
Figure 29. Sound Pressure Levels versus Thrust for 3 Tip Speeds,
CH-3C

53
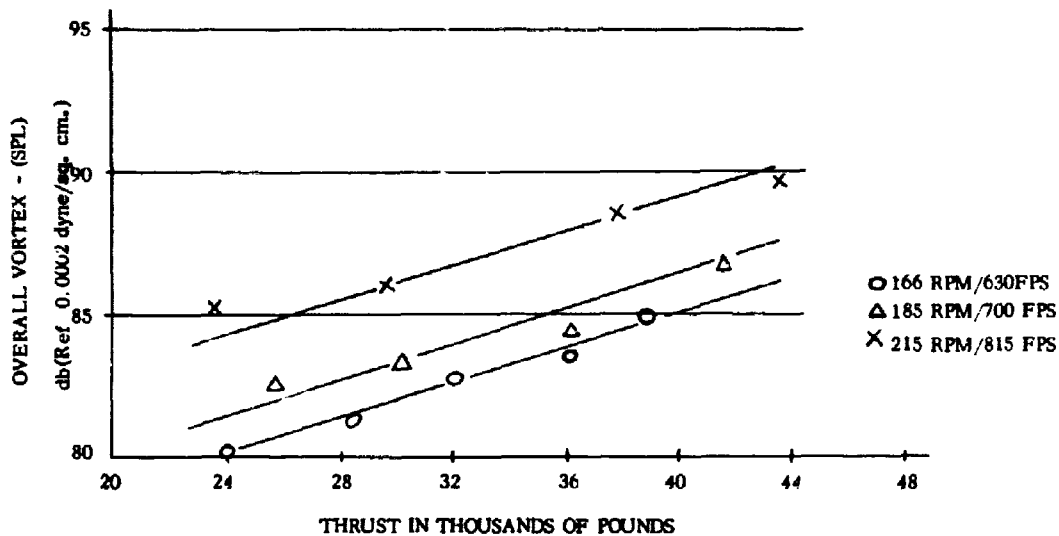
Figure 30. Sound Pressure Levels versus Thrust for 3 Tip Speeds, CH-53A
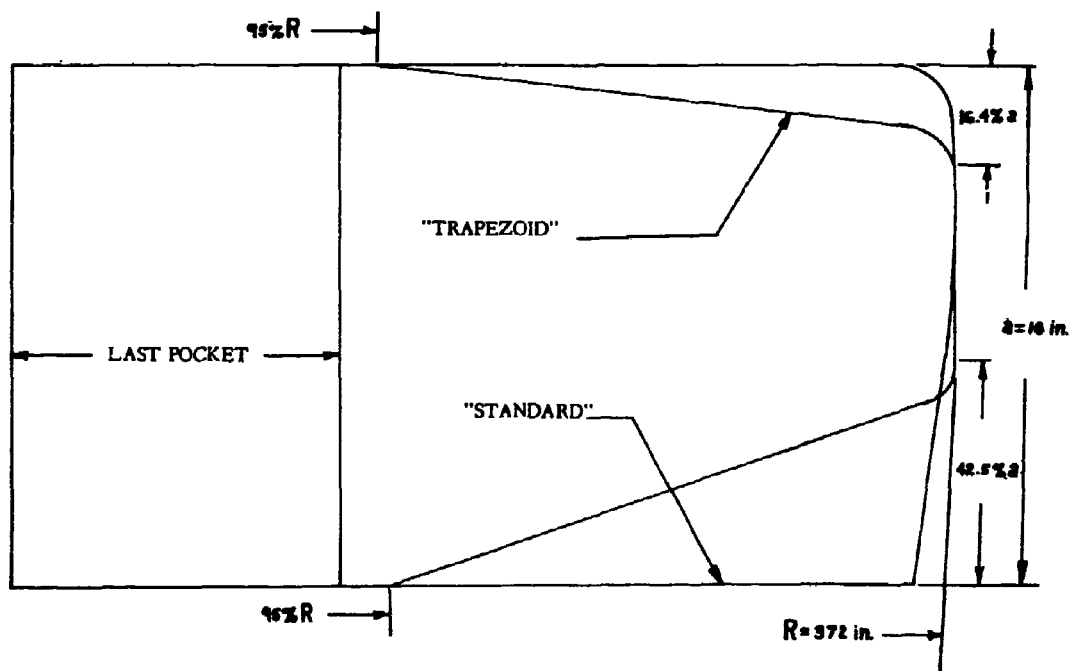
Figure 31. Trapezoidal and Square Tip Planforms
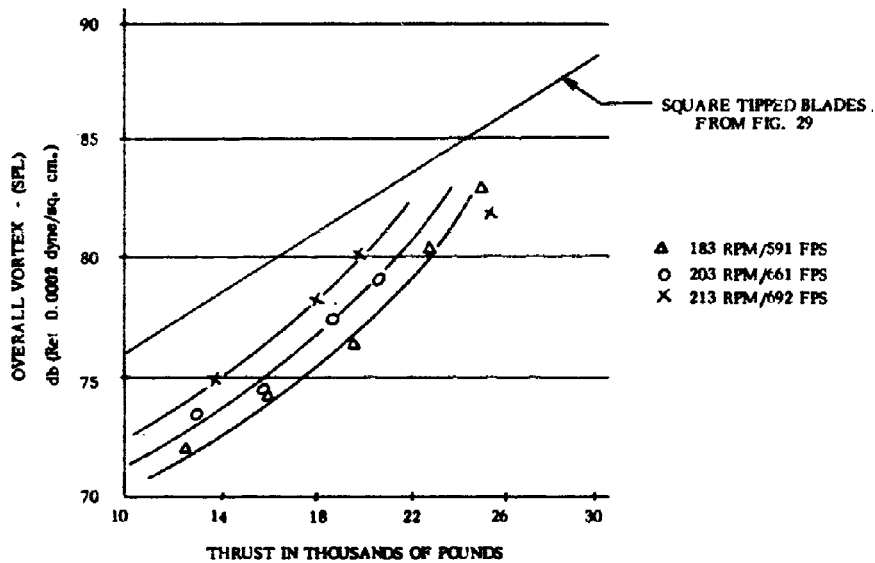
Figure 32. Sound Pressure Level versus Thrust - Trapezoidal
Tips
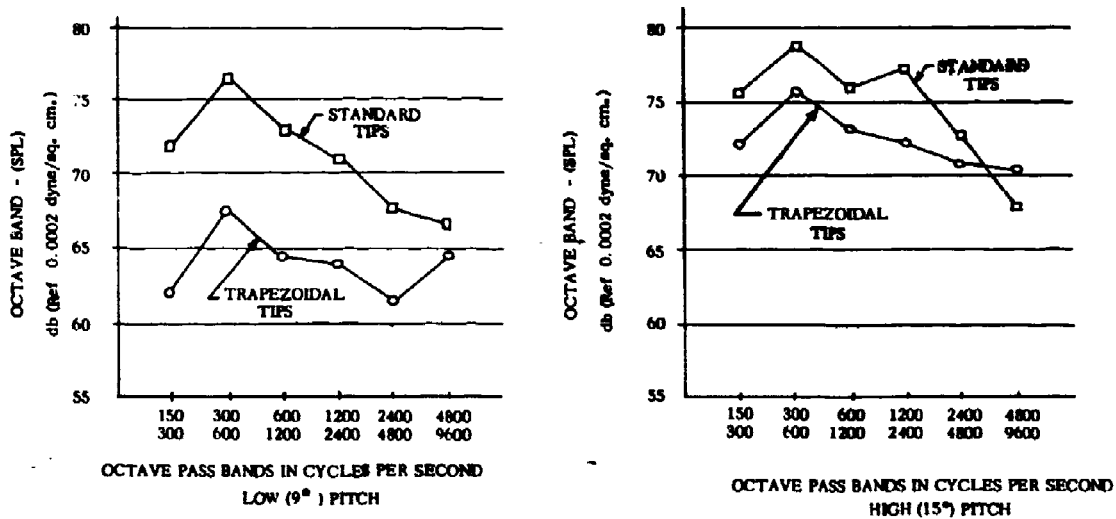
Figure 33. Octave Band Levels for Low and High Pitch (CH-3C)

55
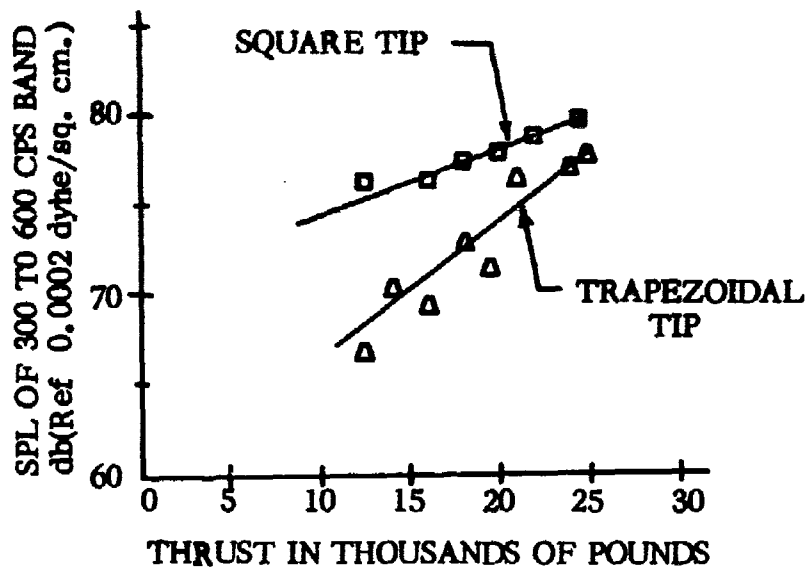
Figure 34. Comparison of Level at Strouhal Frequency of Square and
Trapezoidal Tips @ 203 RPM
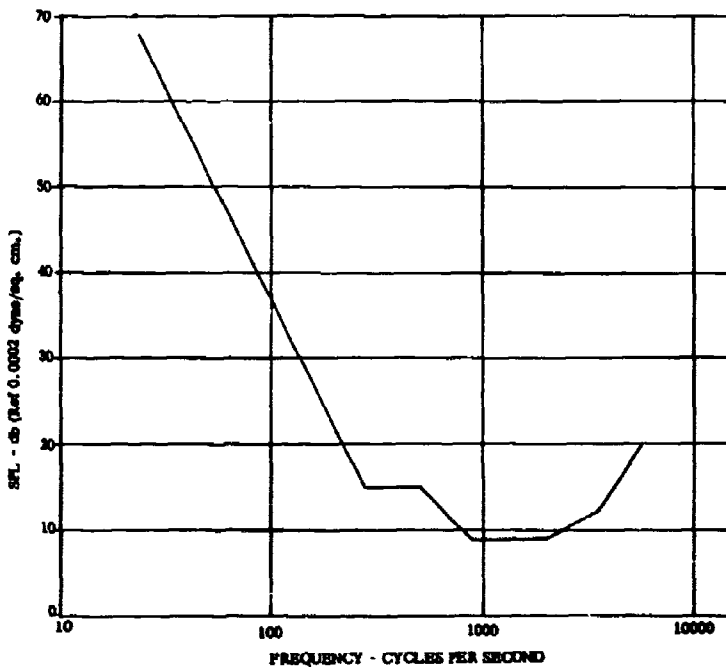
Figure 35. Detection Level Criteria for Aircraft - Spectrum Level

56
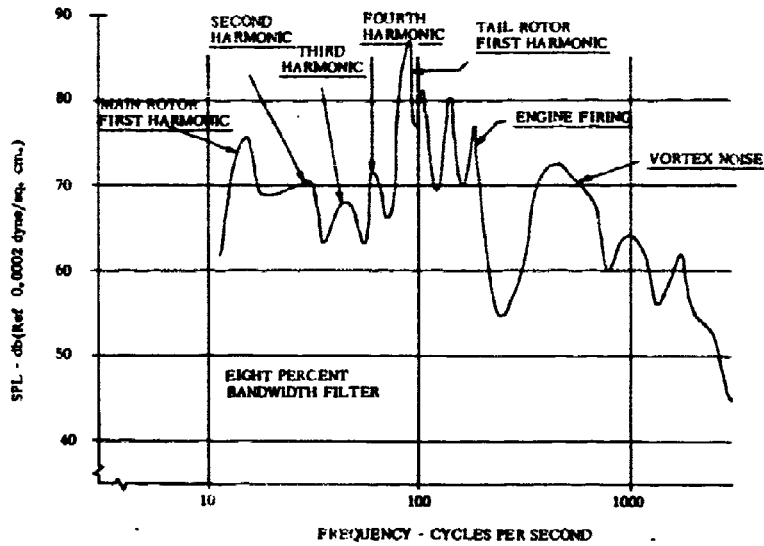
Figure 36. An S-58 Helicopter Noise Spectrum at
Hover

A - LOADING CONCENTRATED IN AN
8-INCH LENGTH OF BLADE

B - LOADING SPREAD OUT OVER
8 FEET OF BLADE

ROTOR DIAMETER IS 48 FEET
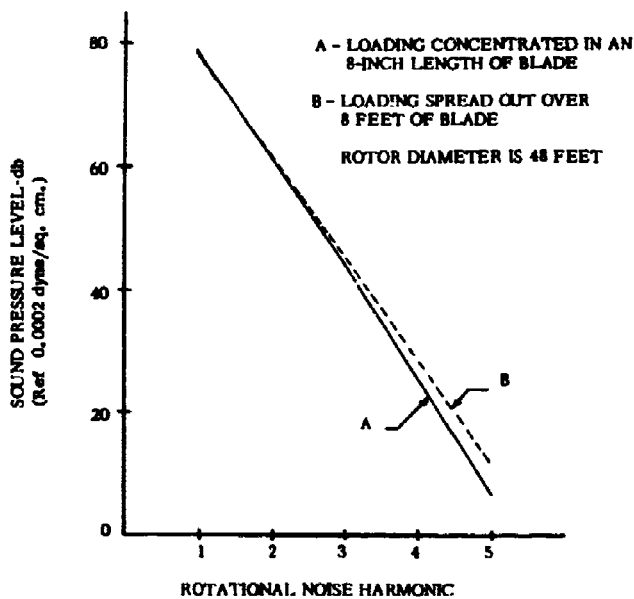
Figure 37.   Effect of Blade Loading Distribution on Noise Harmonic
Level

57
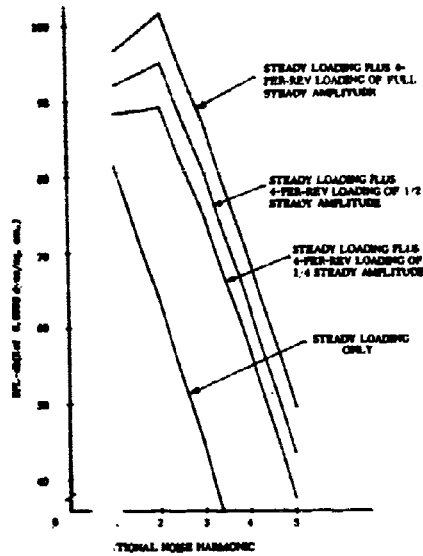
Figure 38. Effect of 4-per-rev Blade Loading on Harmonic Noise Levels
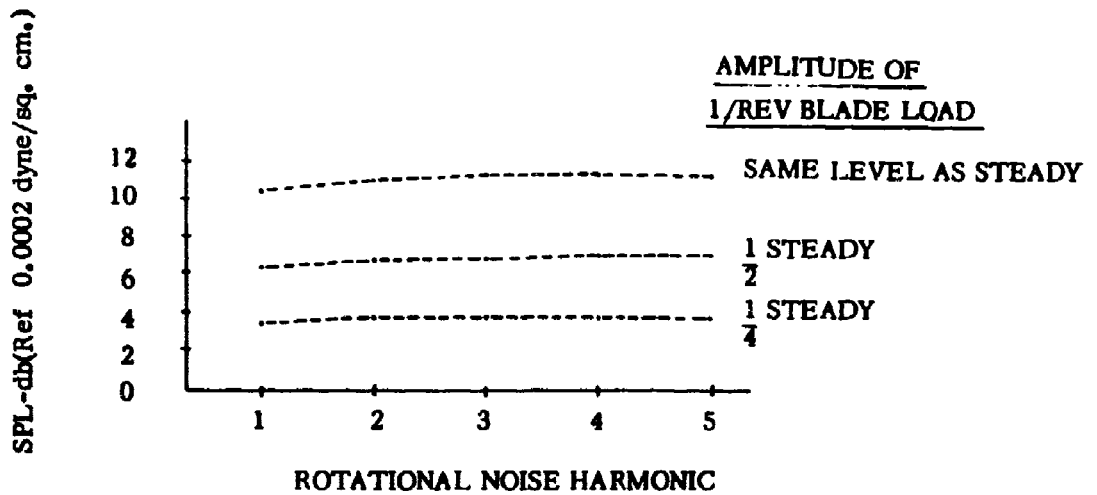
Figure 39. Effect of 1-per-rev Blade Loading on Rotational Noise
Harmonics

58
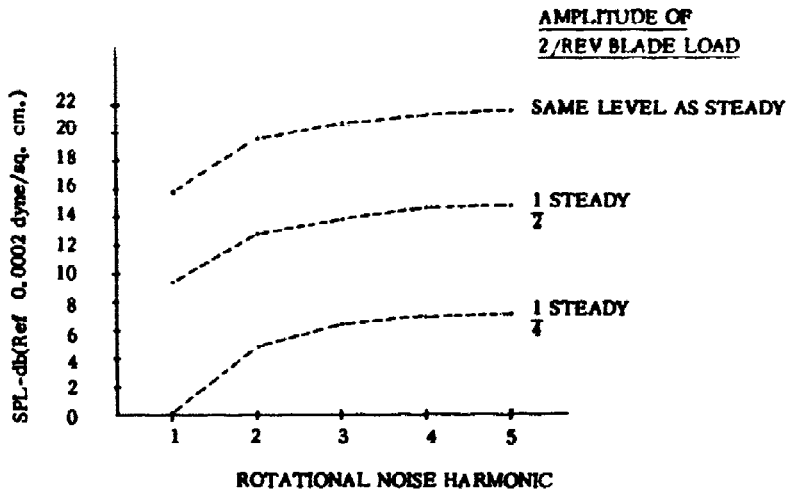
Figure 40. Effect of 2-per-rev Blade Loading on Rotational Noise Harmonics
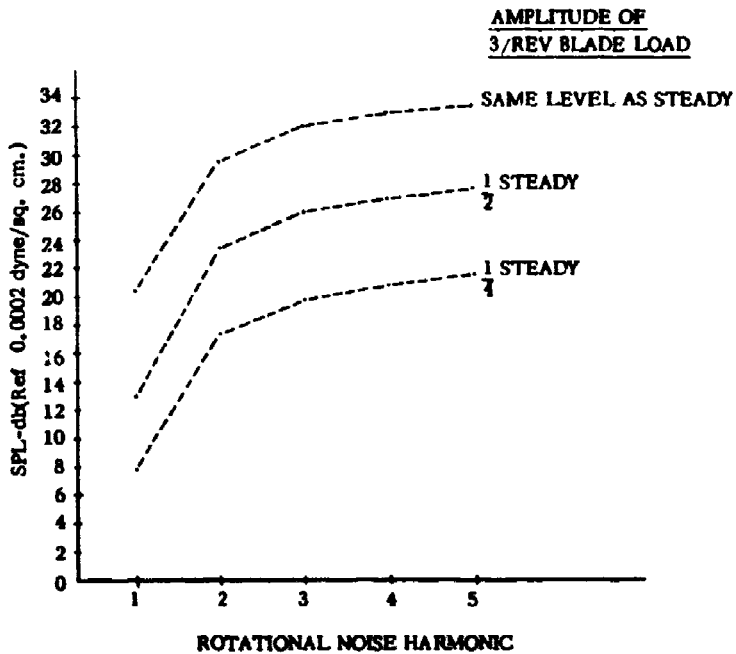
Figure 41. Effect of 3-per-rev Blade Loading on Rotational Noise Harmonics
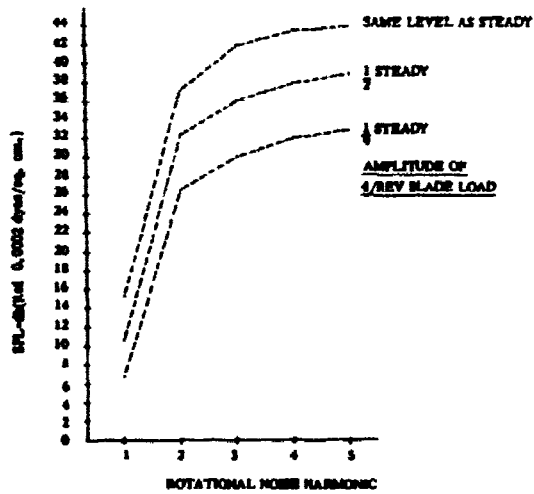
Figure 42. Effect of 4-per-rev Blade Loading on Rotational Noise Harmonics
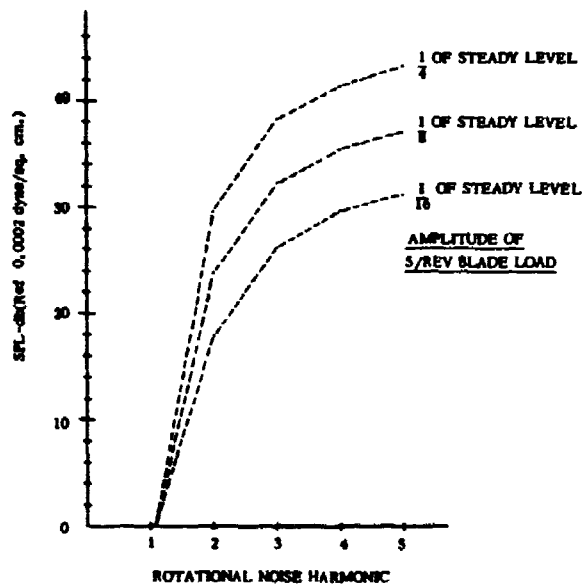
Figure 43. Effect of 5-per-rev Blade Loading on Rotational Noise Harmonics
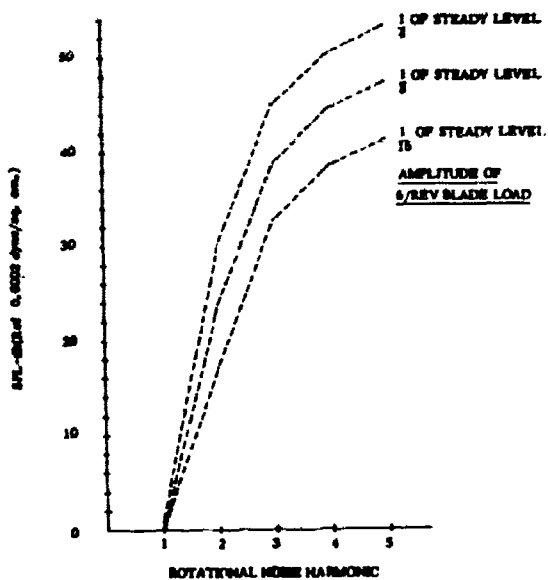
Figure 44. Effect of 6-per-rev Blade Loading on Rotational Noise Harmonics
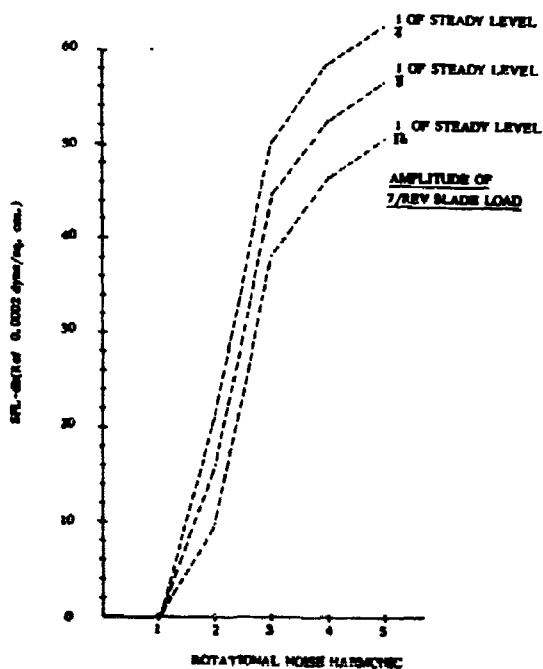
Figure 45. Effect of 7-per-rev Blade Loading on Rotational Noise Harmonics
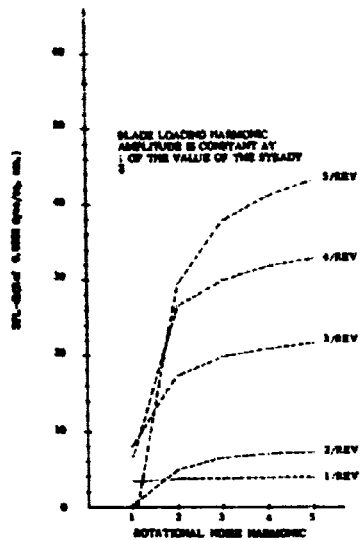
Figure 46. Influence of the 1st to the 5th Blade Loading Harmonics
on Rotational Noise Harmonics
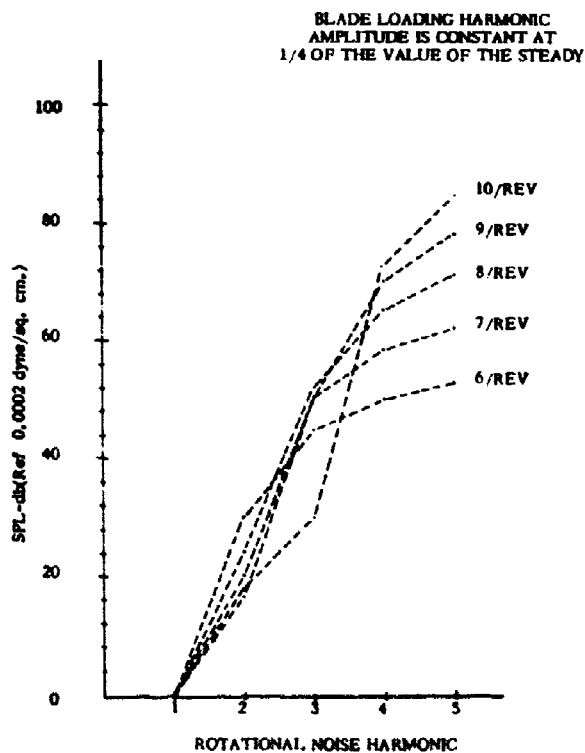
Figure 47. Influence of the 6th to the 10th Blade Loading Harmonics
on Rotational Noise Harmonics
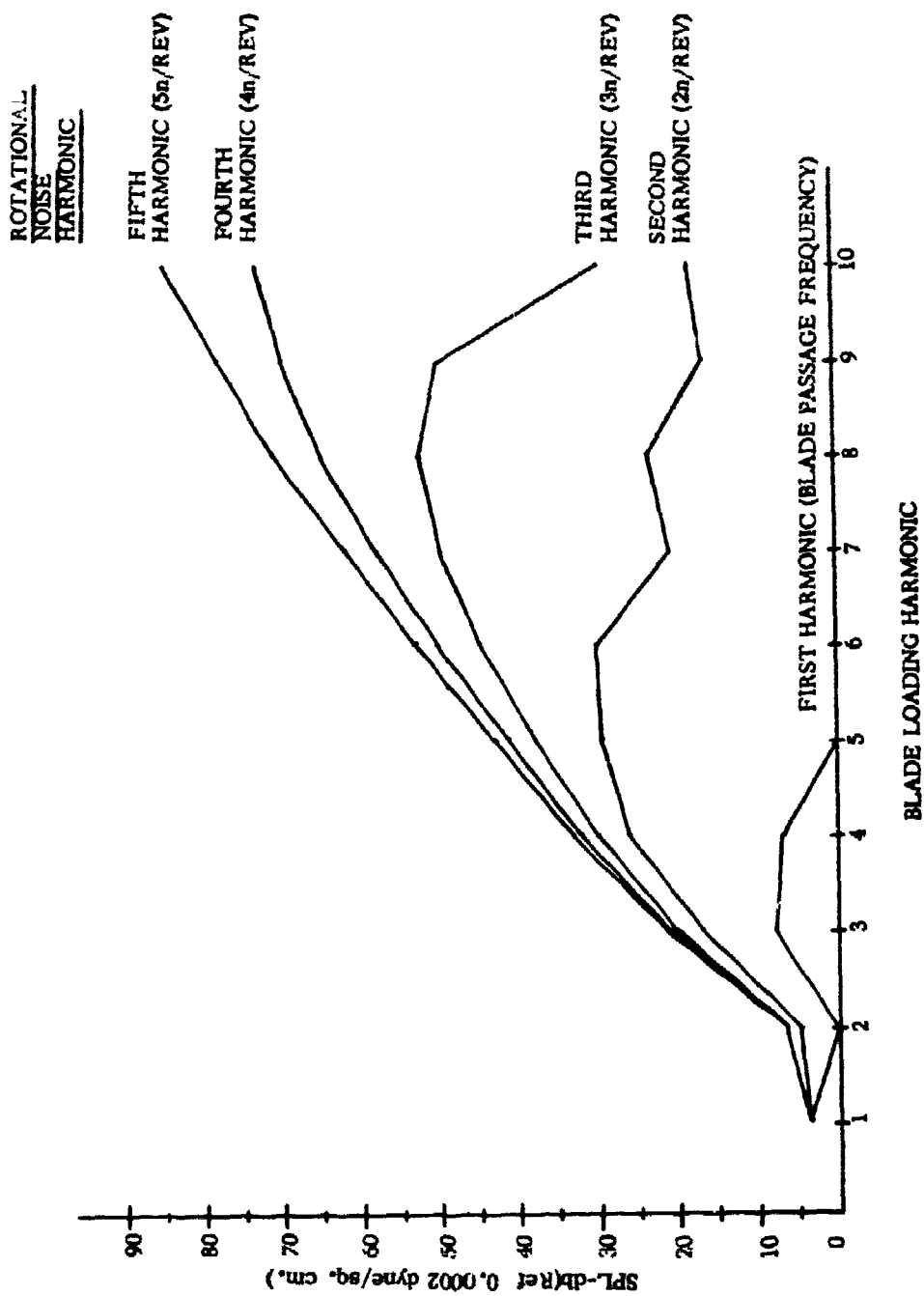
Figure 48. Additional Noise at the First to the Fifth Noise Harmonic Frequencies Due to the Introduction of 1-per-rev to 10-per-rev Harmonic Blade Loadings of One Quarter the Amplitude of the Steady Component
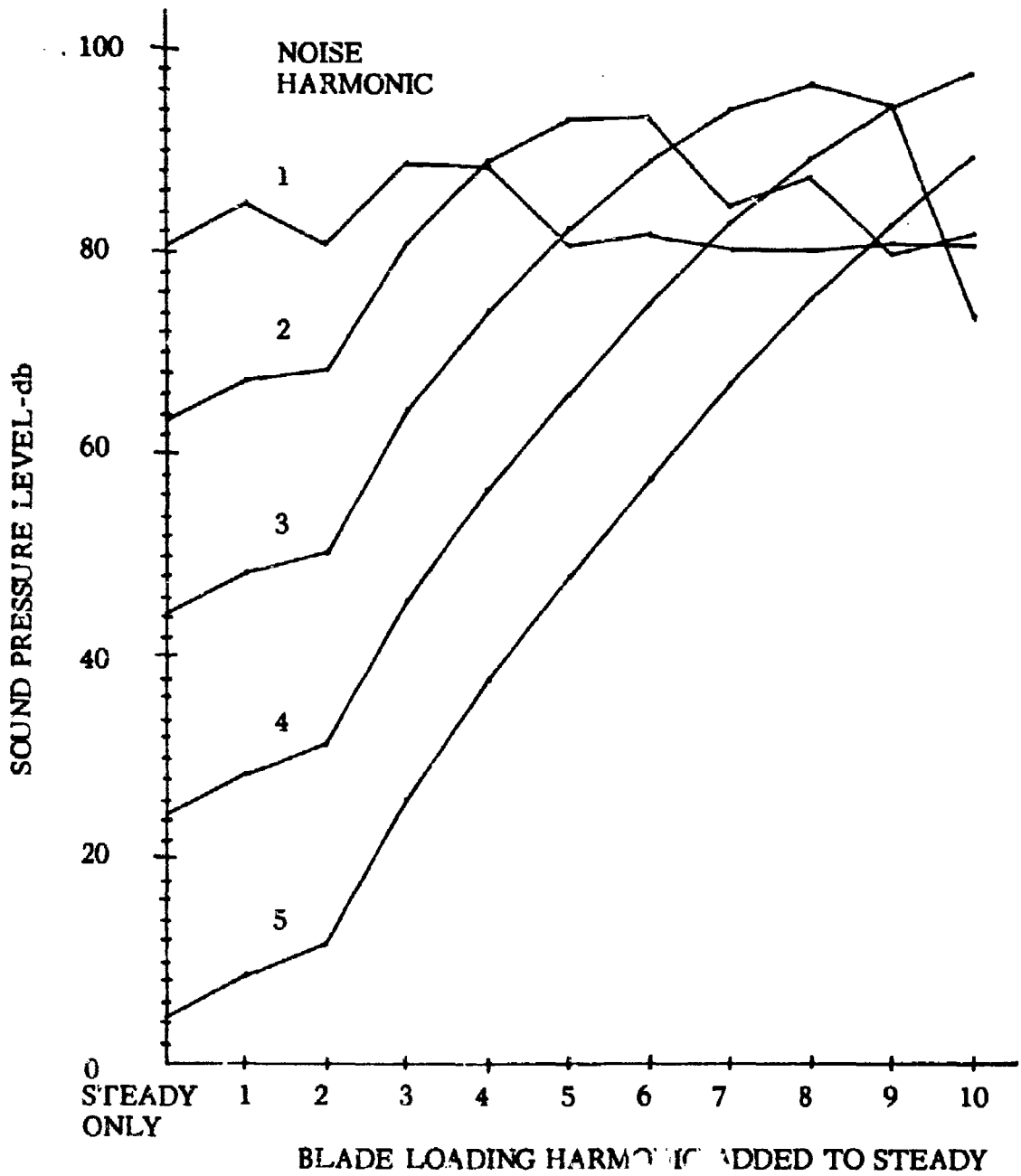
Figure 49. Sound Level Caused by a Rotor wiu ..eady Loading Plus
a Harmonic Blade Loading of One Quarter the Amplitude of the Steady

64

CONCLUSIONS

It as been shown that single rotor overall vortex noise level for square tipped blades with uniform inflow can be calculated with excellent accuracy by the use of a simple formula developed in this study. The standard vortex noise spectrum is used for the unstalled condition, and another spectrum has been developed for use where stall is present. This stall spectrum contains higher levels in the upper frequencies. A reduction in rotor tip speed or thrust, or an increase in blade area (at constant thrust and tip speed) will reduce the overall vortex noise level. Vortex noise level is highly dependent on tip shape, and substantial reductions may be attained by proper design.

The solution derived for rotational noise may be used to calculate any number of harmonics in either the near or the far field under uniform or nonuniform conditions. Only single rotor systems, however, may be considered using the present solution. The only limitation to the number of harmonics that may be calculated appears to be the availability of accurate harmonic blade loading data. Harmonic blade loadings contribute significantly to the fundamental rotational harmonic and for all practical purposes completely determine detectability levels. Low-frequency rotational noise may be reduced by lowering blade loading and rotor speed. High harmonic rotational noise may be reduced by reducing the local stall and drag divergence tendencies of blades and by altering aeroelastic characteristics to minimize harmonic airloads.

Blade slap is a phenomenon which affects both rotational and vortex noise spectra and is generated by rapid changes of flow separation which occur during stall or drag-divergence conditions. Blade tip design is extremely important in attenuating blade slap. The trapezoidal shaped blade tip used in the present study produced significant reductions in blade slap noise level.

RECOMMENDATIONS FOR FURTHER STUDY

1. Conduct an analysis - test correlation program to evaluate the accuracy of the rotor noise analysis using the harmonic airload results of the NH-3A (S-61F) airload measurement program.

2. Undertake further development of existing aeroelastic-aerodynamic programs to extend their capabilities for predicting harmonic blade airloads to higher harmonics.

3. Perform a noise/performance/aeroelastic trade-off on an existing helicopter to define an optimum low-noise configuration. Modify a ship to this configuration for verification of results and for demonstration purposes.

4. Define the relationships between blade slap and the degree of stall, the extent of compressible drag-divergence, and tip vortex characteristics.

BIBLIOGRAPHY

1. Arnoldi, R. A., Propeller Noise Caused by Blade Thickness, United Aircraft Corporation Research Department, Report R-0896-1, East Hartford, Connecticut, January 10, 1956.

2. Bell Helicopter Company, A Study of the Origin and Means of Reducing Helicopter Noise, TCREC Technical Report 62-73, U. S. Army Transportation Research Command*, Fort Eustis, Virginia, November 1962.

3. Carmichael, D., and Mull, H., Recommended Design Trends for Quiet Tail Rotors, Sikorsky Aircraft Report SER-50307, Stratford, Connecticut, September 1962.

4. Curle, N., The Influence of Solid Boundaries Upon Aerodynamic Sound, Proceedings of the Royal Society, A, 231, London, England, 1955.

5. Davidson, I. M., and Hargest, T. J., "Helicopter Noise", Journal of the Royal Aeronautical Society, Volume 69, May 1965.

6. Fletcher, Harvey, and Munson, W. A., Loudness, Its Definition, Measurement, and Calculation, Journal of the Acoustical Society of America, Volume V, October 1933.

7. Garrick, I. E., and Watkins, Charles E., A Theoretical Study of the Effect of Forward Speed on the Free Space Sound-Pressure Field Around Propellers, NACA Report 1198, Langley Field, Virginia, 1954.

8. Gerstenberger, Walter, and Wood, Edward R., Analysis of Helicopter Aeroelastic Characteristics in High Speed Flight, AIAA Journal, Volume I, Number 10, October 1963.

9. Gessow, Alfred, and Myers, Gerry C., Jr., Aerodynamics of the Helicopter, First Printing, The Macmillan Company, New York, 1952.

10. Gustafson, F. B., and Myers, G. C., Jr., Stalling of Helicopter Blades, NACA TM 1083, Washington, D. C., 1946.

---

* Now U. S. Army Aviation Materiel Laboratories.

11. Gutin, L., On the Sound Field of a Rotating Propeller, NACA TM 1195, Washington, D. C., October 1948.

12. Hicks, Chester W., and Hubbard, Harvey H., Comparison of Sound Emission From Two-Blade, Four-Blade, and Seven-Blade Propellers, NACA Technical Note 1354, Washington, D. C., July 1947.

13. Hubbard, Harvey H., and Maglieri, Domenic J., An Investigation of Some Phenomena Relating to Aural Detection of Airplanes, NACA Technical Note 4337, Washington, D. C., September 1958.

14. Hubbard, Harvey H., and Regier, Arthur A., Free Space Oscillating Pressures Near the Tips of Rotating Propellers, NACA Report 996, Washington, D. C., 1950.

15. Hubbard, Harvey H., and Regier, Arthur A., Propeller Loudness Charts for Light Airplanes, NACA Technical Note 1358 Washington, D. C., July 1947.

16. Hubbard, Harvey H., Propeller-Noise Charts for Transport Airplanes, NACA Technical Note 2968, Washington, D. C., June 1953.

17. Ingard, Uno, Sound Radiation from a Propeller in a Nonuniform Medium, Pratt & Whitney Aircraft, East Hartford, Connecticut, January 1964.

18. Lamb, H., Hydrodynamics, Sixth Edition, Cambridge University Press, London, England, 1932.

19. Lighthill, M. J., Sound Generated Aerodynamically, Proceedings of the Royal Society, A 211, London, England, 1952.

20. Loewy, R. G., Aural Detection of Helicopters in Tactical Situations, Part II, Institute for Defense Analysis Research Paper P-25, AD 409535, Alexandria, Virginia, May 1963.

21. Miller, R. H., Rotor Blade Harmonic Air Loading, IAS Paper No. 62-82, January 1962.

22. Mull, H. R., External Noise Characteristics of Two Commercial Transport Helicopters, United Acoustic Consultants Report R-642 and Addendum, Wilton, Connecticut, January 23, 1964.

23. Oestreicher, Hans L., "Field of a Spatially Extended Moving Sound Source", Journal of the Acoustical Society of America, Volume 29, Number 11, New York, N. Y., November 1957.

24. Piziali, R., and DuWaldt, F., A Method for Computing Rotary Wing Airload Distribution in Forward Flight, TREC Technical Report 62-44, U. S. Army Transportation Research Command, Fort Eustis, Virginia, July 1962.

25. Piziali, R., and DuWaldt, F., Computation of Rotary Wing Harmonic Airloads and Comparison with Experimental Results, American Helicopter Society, New York, New York, May 1962.

26. Powell, Alan, "Theory of Vortex Sound", The Journal of the Acoustical Society of America, Volume 36, Number 1, January 1964.

27. Roberts, John P., and Beranek, Leo L., Experiments in External Noise Reduction of a Small Pusher-Type Amphibian Airplane, Washington, D. C. NACA TM 2727, July 1952.

28. Roshko, Anatol, Experiments on the Flow Past a Circular Cylinder at Very High Reynolds Number, Journal of Fluid Mechanics, Volume 10, Part 3, May 1961.

29. Scheiman, James, A Tabulation of Helicopter Rotor-Blade Differential Pressures, Stresses, and Motions as Measured in Flight, NASA TM X-952, Langley Station, Hampton, Virginia, March 1964.

30. van de Vooren, A. I., and Zandbergen, P. J., Noise Field of a Rotating Propeller in Forward Flight, AIAA Journal, Volume 1 No. 7, July 1963.

31. Watkins, Charles E., and Durling, Barbara J., A Method for Calculation of Free-Space Sound Pressures Near a Propeller in Flight Including Considerations of a Chordwise Blade Loading, NACA TM 3809, Washington, D. C., 1956.

32. Wood, E. R., and Hilzinger, K. D., A Method for Determining the Fully Coupled Aeroelastic Response of Helicopter Rotor Blades, Presented at the American Helicopter Society Nineteenth Annual National Forum, Washington, D. C., May 1 - 4, 1963.

33. Yudin, E. Y., On the Vortex Sound From Rotating Rods, NACA TM No. 1136, Washington, D. C., March 1947.

34. Zandbergen, P. J., and van der Walle, F., On the Calculation of the Propeller Noise Field Around Aircraft, National Aero and Astronautical Research Institute, Amsterdam, Netherlands, NLR TM G-23, 1962.

Items 3 and 17 are not to be considered as subject data required to be furnished under this contract but are merely references that can be made available to the government on a limited rights basis.

DISTRIBUTION

US Army Materiel Command	5
US Army Aviation Materiel Command	6
US Army Aviation Materiel Laboratories	23
US Army Limited War Laboratory	1
US Army Human Engineering Laboratories	1
US Army Research Office-Durham	1
US Army Test and Evaluation Command	1
Plastics Technical Evaluation Center	1
US Army Medical R&D Command	1
US Army Combat Developments Command, Fort Belvoir	2
US Army Combat Developments Command Transportation Agency	1
US Army Combat Developments Command Experimentation Command	3
US Army War College	1
US Army Command and General Staff College	1
US Army Aviation School	1
US Army Tank-Automotive Center	2
US Army Electronics Command	2
US Army Aviation Test Activity, Edwards AFB	2
Air Force Flight Test Center, Edwards AFB	2
US Army Field Office, AFSC, Andrews AFB	1
Systems Engineering Group (RTD), Wright-Patterson AFB	1
Air Force Flight Dynamics Laboratory, Wright-Patterson AFB	1
Naval Air Systems Command	5
Chief of Naval Research	3
US Naval Research Laboratory	1
Marine Corps Liaison Officer, US Army Transportation School	1
Testing and Development Division, US Coast Guard	1
Manned Spacecraft Center, NASA	1
NASA Scientific and Technical Information Facility	2
NAFEC Library (FAA)	2
US Army Aviation Human Research Unit	2
US Army Board for Aviation Accident Research	1

Bureau of Safety, Civil Aeronautics Board	2
US Naval Aviation Safety Center, Norfolk	1
Federal Aviation Agency, Washington, D. C.	2
CAMI Library, FAA	1
Defense Documentation Center	20

APPENDIX I

SAMPLE CALCULATION OF VORTEX SOUND LEVELS

The vortex noise levels are easily calculated by use of equation 6 and the vortex sound spectra in Figure 1.

Using the CH-3C blade system operating at 203 rpm and producing a thrust of 19,000 pounds for our calculations, the system parameters listed in Table III are used.

Equation 6 is used to obtain the SPL at 300 feet.

$$SPL = 10 \log \frac{6.1 \times 10^{-27} A_B (V_{0.7})^6}{10^{-16}} + 20 \log \frac{C_L}{0.4}$$

From Table III

$$A_B = 217$$

Since for this configuration the drag is small compared to the lift ($C_D = 0.077$), it is assumed that the lift is approximately equal to the thrust.

Then $\quad C_L = \dfrac{2T}{\rho A_B (V_{0.7})^2}$ $\qquad$ (Reference 16)

Substituting the given values

$$C_L = \frac{(19,000)^2}{(0.002378)(217)(463)^2}$$

$$C_L = 0.35$$

Substituting these values in equation 6,

$$SPL = 10 \log \frac{6.1 \times 10^{-27} (217)(463)^6}{10^{-16}} + 20 \log \frac{0.35}{0.4}$$

$$SPL = 10 \log 1.3 \times 10^8 + 20 \log 0.875$$

$$SPL = 81.2 - 0.4$$

$$SPL = 80.8 \ @ \ 300 \ feet$$

To correct to distances of other than 300 feet from the rotor, utilize the expression

$$\Delta SPL = 20 \log \frac{300}{R}$$

In this case we wish to obtain the level at 225 feet to compare with measured data.

$$\Delta SPL = 20 \log \frac{300}{225}$$

$$\Delta SPL = 2.6 \, db$$

Applying this correction to the level at 300 feet, we obtain

$$SPL = 80.8 + 2.6 \quad \text{or} \quad 83.4 \text{ @ } 225 \text{ feet}$$

Since the operating range is below stall on the drag-divergence curve of Figure 21, the spectrum of Figure 19 should be used. With a calculated overall vortex level of 83 db at 225 feet, the spectrum is then predicted to be as follows:

Octave Band (CPS)	SPL (db Ref. 0.0002 dyne/sq. cm.)
150-300	75.0
300-600	79.0
600-1200	75.0
1200-2400	74.5
2400-4800	70.5
4800-9600	66.0

The measured values for this condition were:

150-300	75.0
300-600	78.0
600-1200	74.0
1200-2400	74.5
2400-4800	70.5
4800-9600	66.0

The overall level for the measured noise can be obtained by combining the octave band levels logarithmically. To obtain the overall SPL from octave band levels, first determine the intensity ratios of the individual octaves.

$$SPL_1 = 10 \log \frac{I_1}{I_0} \qquad \frac{I_1}{I_0} = 10^{\left(\frac{SPL_1}{10}\right)}$$

$$SPL_2 = 10 \log \frac{I_2}{I_0} \qquad \frac{I_2}{I_0} = 10^{\left(\frac{SPL_2}{10}\right)}$$

Sum the intensity ratios to obtain the overall intensity ratio.

$$\frac{I_T}{I_0} = \frac{I_1}{I_0} + \frac{I_2}{I_0} + \cdots$$

Convert to overall SPL.

$$SPL = 10 \log \frac{I_T}{I_0}$$

The results are summarized below:

Octave Band (CPS)	SPL (db) Measured	Calculated
Overall	82.0	83.0
150-300	75.0	75.0
300-600	78.0	79.0
600-1200	74.0	75.0
1200-2400	74.5	74.5
2400-4800	70.5	70.5
4800-9600	66.0	66.0

APPENDIX II

VORTEX NOISE TEST INSTRUMENTATION

A block diagram of the instrumentation used in the test program is presented in Figure 50. The acoustic signal was picked up with a low impedance moving-coil microphone. The microphone was coupled to a General Radio 1551-C Sound Level Meter which served as a calibrated pre-amplifier and decade attenuator. The output of the sound level meter was recorded on a Nagra III B tape recorder. The overall system was calibrated electrically prior to each series of measurements.
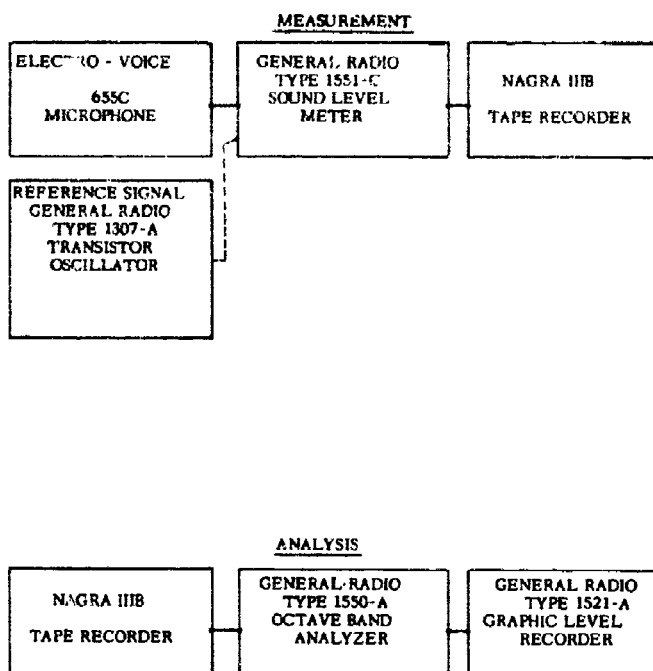
MEASUREMENT

| ELECTRO - VOICE 655C MICROPHONE | GENERAL RADIO TYPE 1551-C SOUND LEVEL METER | NAGRA IIIB TAPE RECORDER |

| REFERENCE SIGNAL GENERAL RADIO TYPE 1307-A TRANSISTOR OSCILLATOR |

ANALYSIS

| NAGRA IIIB TAPE RECORDER | GENERAL RADIO TYPE 1550-A OCTAVE BAND ANALYZER | GENERAL RADIO TYPE 1521-A GRAPHIC LEVEL RECORDER |

Figure 50.   Vortex Noise Test
Instrumentation

The recorded data was played back through an octave band analyzer. The octave band levels were recorded with a graphic level recorder. Because of the rapidly changing position of the rotating source and the proximity of the microphone with respect to the source, each of the octave bands showed short time variations or modulation. In addition, there were longer time variations that were attributed to changing wind conditions. These time variations were averaged out by graphically recording the levels of the individual octaves and noting the midpoint of the spread. The modulation was found to be higher at the lower end of the spectrum than at the high-frequency end of the spectrum.

The time-averaged data was then corrected for system response and the octave band levels were tabulated. The overall vortex noise level was computed by summing the corrected levels in the individual octaves from the 150-300 cps band to the 4800-9600 cps band.

76

APPENDIX III

CALCULATION OF PARTIAL DERIVATIVES

Calculate $\frac{\partial S}{\partial x}$ knowing

$$S^2 = R^2 + r^2 - 2rR\cos\sigma(\cos\theta\cos\psi + \sin\theta\sin\psi) \qquad (29)$$

From Figure 3

$$R^2 = x^2 + y^2 + z^2 \quad , \quad \cos\theta = \frac{x}{-R\cos\sigma} \quad , \quad \sin\theta = \frac{y}{R\cos\sigma}$$

Therefore, write

$$S^2 = x^2 + y^2 + z^2 + r^2 - 2r\cos\sigma\frac{x^2+y^2+z^2}{(x^2+y^2+z^2)\cos\sigma}(x\cos\psi + y\sin\psi) \qquad (30)$$

which reduces to

$$S^2 = x^2 + y^2 + z^2 + r^2 - 2r(x\cos\psi + y\sin\psi) \qquad (31)$$

Taking the partial with respect to x

$$S\frac{\partial S}{\partial x} = x + r\cos\psi \qquad (32)$$

but noting that $x = -R\cos\sigma\cos\theta$ this reduces to

$$\frac{\partial S}{\partial x} = \frac{-R}{S}\cos\sigma\cos\theta + \frac{r}{S}\cos\psi \qquad (33a)$$

Similarly, for the y and z directions

$$\frac{\partial S}{\partial y} = \frac{R}{S}\cos\sigma\sin\theta - \frac{r}{S}\sin\psi \qquad (33b)$$

$$\frac{\partial S}{\partial z} = \frac{R}{S}\sin\sigma \qquad (33c)$$

77

It is desirable to eliminate the second term of Equations (33a) and (33b) in order to simplify the solution. From the ratio of magnitudes of the two terms it appears that this elimination may be valid if the field point distance R is one diameter or more.

Equation (33) then becomes

$$\frac{\partial S}{\partial x} = \frac{-R}{S} \cos \sigma \cos \theta$$

$$\frac{\partial S}{\partial y} = \frac{R}{S} \cos \sigma \sin \theta$$

$$\frac{\partial S}{\partial z} = \frac{R}{S} \sin \sigma$$

APPENDIX IV

APPROXIMATION OF CHORDWISE PRESSURE DISTRIBUTION AS A STEP FUNCTION PLUS SCALE SHIFT

The Fourier series expansion of the initial blade passage time history in the rotor disk (Figure 5) is

$$\Delta P(r,\Psi,t) = \sum_{m=1}^{\infty} A_m \cos mn\Omega t + B_m \sin mn\Omega t$$

where

$$A_m = \frac{n\Omega}{\pi} \int_{\Psi/\Omega}^{\Psi/\Omega + 2\pi/n\Omega} \Delta P(r,\Psi,t) \cos mn\Omega t \, dt \tag{34a}$$

$$B_m = \frac{n\Omega}{\pi} \int_{\Psi/\Omega}^{\Psi/\Omega + 2\pi/n\Omega} \Delta P(r,\Psi,t) \sin mn\Omega t \, dt \tag{34b}$$

By shifting the time scale by Ψ/Ω the pressure pulse appears as in Figure 51. The corresponding mathematical representation is

$$\Delta P(r,\Psi,t) = \sum_{m=1}^{\infty} a_m \cos(mn\Omega t - mn\Psi) + b_m \sin(mn\Omega t - mn\Psi)$$

with

$$a_m = \frac{n\Omega}{\pi} \int_{0}^{2\pi/n\Omega} \Delta P(r,\Psi,T + \Psi/\Omega) \cos mn\Omega T \, dT \tag{35a}$$

$$b_m = \frac{n\Omega}{\pi} \int_{0}^{2\pi/n\Omega} \Delta P(r,\Psi,T + \Psi/\Omega) \sin mn\Omega T \, dT \tag{35b}$$

where

$$T = t - \Psi/\Omega$$

As an approximation to the function of Figure 51, a step function will be used as shown in Figure 52. The amplitude of this step function is

$$\overline{\Delta P} = \int_{0}^{a/\Omega r} \frac{\Delta P(r,\Psi,t)}{a/\Omega r} \, dt \tag{36}$$

An additional scale shift of $a/2\Omega r$ permits expansion of the function of Figure 52 as a cosine series and gives

$$\Delta P(r, \mathcal{V}, t) = \sum_{m=1}^{\infty} a_m \cos\left(mn\Omega t - mn\mathcal{V} - \frac{man}{2r}\right) \qquad (37)$$

where

$$a_m = \frac{2}{m\pi} \sin\frac{man}{2r} \overline{\Delta P}$$

which corresponds to the function of Figure 6.
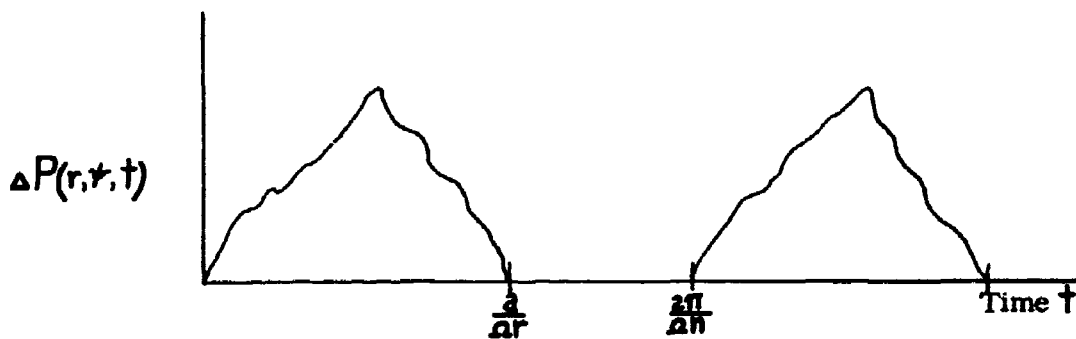
Figure 51. Time History of Blade Passage Over $r \, dr \, d\mathcal{V}$ After Time Shift
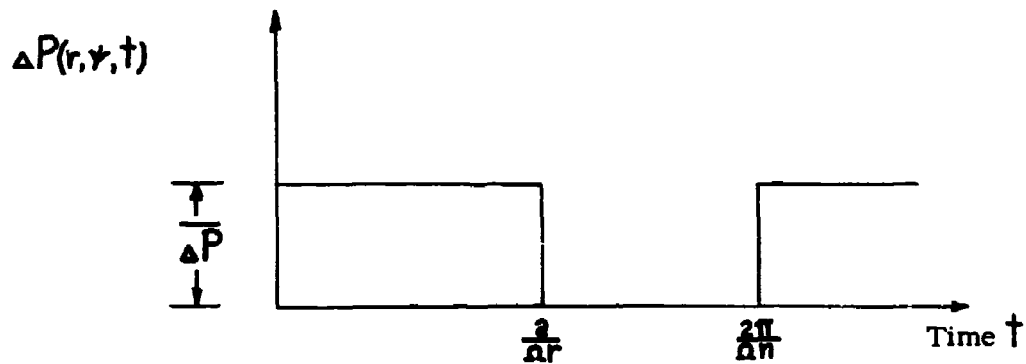
Figure 52. Step Function Approximation

80

APPENDIX V

DEFINITION OF BLADE PITCH ANGLE

Blade angle β is controlled by collective pitch, cyclic pitch, and twist. With the coordinate system of Figure 2, the following is true:

longitudinal cyclic pitch angle = $\beta_1 \cos \Psi$

lateral cyclic pitch angle = $\overline{\beta_1} \sin \Psi$

where β_1 and $\overline{\beta_1}$ are the longitudinal and lateral cyclic pitch magnitudes, respectively. The effect of negative blade twist is accounted for as follows:

pitch angle change due to twist = $-\gamma (r - r_0)$

where

γ is the twist rate

r_0 is the blade radial station at which twist begins.

The expression for pitch angle resulting from twist is based on the assumption that the collective pitch angle is measured at the blade root. Combining the effects of cyclic pitch, twist effect, and β_0 the collective pitch angle, the true blade pitch angle is obtained.

$$\beta = \beta_0 - \gamma(r - r_0) + \beta_1 \cos \Psi + \overline{\beta_1} \sin \Psi$$

APPENDIX VI

DESCRIPTION OF PROGRAM FOR CALCULATING ROTATIONAL NOISE

A program has been developed to facilitate the calculation of rotor rotational noise from equation 26 of this report. This is a Fortran IV program intended for use on the IBM 7094/44 D. C. S. As explained previously, the solution represents sound pressure at a point for rotational noise at the mth harmonic of blade passage. The solution may be used for calculating the rms sound pressure at any point in the near or far field outside one diameter from the rotor. The solution's accuracy decreases with increasing rotor system translational speed up to Mach 0.3 which is the practical limit for accuracy.

Method and Subprograms

The method used repeatedly evaluates the basic sound pressure equation given in the analysis. This includes a double integration. One integration is around the rotor disk with the sample points (azimuth angles) chosen at constant intervals. Subroutine SIMCOR, which used Simpsons (1/3) Rule with correction term was chosen to perform this integration. The other integration is along the radius where sample radial stations are unevenly spaced, hence, requiring the use of subroutine AVQUAD. This is a method whereby several intervals are approximated by "averaged quadratics" and integrated analytically. The flow diagram is shown in Figure 53.

Running time can be approximated at 20 sec. plus 5 sec. per field point. 5,000 units of output is sufficient unless several causes are run with all output options on. The deck setup is as follows:

\$ DCID	with facility accounting information
\$ EXECUTE	IBJOB
\$ IBJOB	MAP

Binary Deck	Rotational Noise
Binary Deck	SIMCOR
Binary Deck	AVQUAD

7/8 END OF JOB

DATA
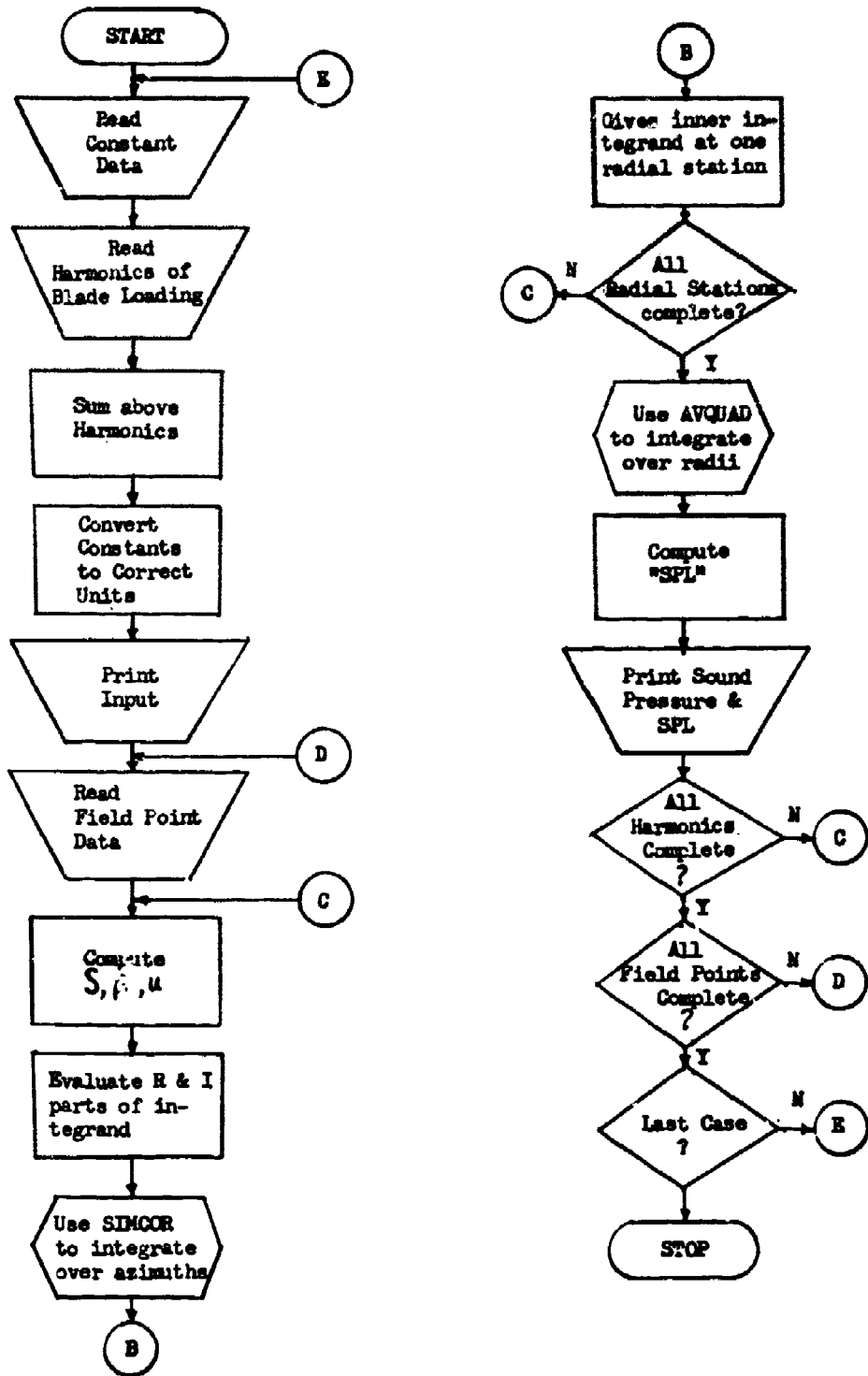
Figure 53. Computer Flow Diagram

83

7/8 END OF JOB

$ IBSYS

$ PAUSE

$ PAUSE

Program Parameters

The parameters which must be known to use the program and their units are listed below:

n Number of rotor blades

Ω Angular velocity of rotor, revolutions per minute

a Blade chord, inches

c Velocity of sound, feet per second

R_0 Radius at start of blade twist, inches

β_0 Collective (steady) pitch angle, degrees

β_1 Cosine component of cyclic pitch (longitudinal), degrees

$\bar{\beta_1}$ Sine component of cyclic pitch (lateral), degrees

γ Blade twist rate, degrees per inch

L_0 Steady blade section loading for one radial station, pounds per inch

L_m Cosine component of the mth harmonic of blade section loading for one radial station, pounds per inch

M_m Sine component of the mth harmonic of blade section loading for one radial station, pounds per inch

R Distance from center of rotor to point at which noise level is to be calculated, feet

84

θ Angle in rotor plane between longitudinal axis of helicopter (0 degrees at tail) and point at which level is to be calculated, positive in direction of rotor rotation, degrees

σ Angle in plane of rotor axis between rotor plane and point at which level is to be calculated, positive in direction of rotor thrust, degrees

Figures 2 and 3 show system parameters.

Input Format

The input format, which is to be used for every case is described below. The input format is shown on the coding form in Figure 54. A sample case is shown in Figure 55.

Card 1: Title Card

     Col. 1 - 1, Col. 2 - any desired title

Card 2: Basic Constants

     Col. 2 - end code = 0 last case; = 1 case(s) follow

     Col. 3 & 4 - (right adjusted) number of field points

     Col. 5-12* - n

     Col. 13-20* - Ω

     Col. 21-28* - a

     Col. 29-36* - c

     Col. 37-44* - R_o

     Col. 45-52* - β_o

     Col. 53-60* - β_1

     Col. 61-68* - $\overline{\beta_1}$

     Col. 69-76* - γ

*Must have decimal point.

SIKORSKY TRANSCRIPT SHEET

TITLE *Input Format*

ORIGINATOR _____ EXT. ___

PAGE ___ OF ___

DATE ___

CARD 1

COL 1-72 ANY TITLE INFORMATION

CARD 2

RBW   OMG   CH   SOS   RO   BOI   BI   BII
No. of field points
End code

CARD 3

ΔY
No. of radial station
No. of harmonic

CARD 4   OUTPUT CONTROLS

LOADING DATA (A SET FOR EACH RADIAL STATION)

L_0
L_1 L_b L_{ij}
M_1 M_3 M_{ij}

FIELD POINT DATA

CAPR   THETA   ALFA

Figure 54. Input Format

Figure 55 a. Sample Input Sheet

SIKORSKY TRANSCRIPT SHEET   TITLE *Rotor Noise Prediction*

ORIGINATOR _____ EXT. _____   PAGE *1* OF *2*   DATE _____

```
80 KNOT CRUISE DATA 6 S8 NASA TM X 952 TABLE 13
0 1   4.0   214.0   16.0   1126.0   50.0   13.08   2.21   -5.28   0.024
4 8 2.0
200000
84.0   134.5   185.0   262.0   286.0   362.0   319.0   336.0
2.195
-1.949   .645   -.322   -.070   -.048    .061   -.024    .025    .063    .027
 2.157   -.730   .414    .026   -.074    .080   -.039   -.011   -.034   -.019
6.841
-2.083   1.573   -.082   -.053   -.014   -.002   -.055    .094   -.081   -.093
 3.207   -.608    .380   -.171   -.162   -.140   -.000   -.029   -.105   -.083
9.111
-1.512   2.028    .252   -.018    .123    .162   -.011    .044    .000   -.012
 3.186   -.115    .599    .017   -.198   -.100   -.007   -.037    .051   -.053
17.875
-.217   3.331   1.153    .237    .028    .204    .289   -.215   -.111    .101
-.514   1.147    .677   -.573   -.337   -.006    .123    .026   -.160   -.162
18.889
 1.820   3.068   2.156    .663   -.177    .339   -.060    .126    .083   -.417
-2.687    .370    .047   -.303   1.188    .06     .301   -.393   -.220    .178
```

87

SIKORSKY TRANSCRIPT SHEET

ORIGINATOR _____ EXT. _____

TITLE *Rotor Noise Prediction*

DATE _____

19.036									
3.158	2.307	1.894	1.064	-.130	.181	-.160	-.056	.044	-.021
-3.888	.159	-.122	.028	-1.180	-.277	.415	.036	-.214	-1.041
19.356									
3.608	1.616	1.622	1.242	-.128	.190	.007	-.334	-.038	.503
-3.201	-.013	-.415	.512	-.772	-.758	.395	.553	-.369	-.349
0.0									
0.0	0.0	0.0	0.0	0.0	0.0	0.0	0.0	0.0	
0.0	0.0	0.0	0.0	0.0	0.0	0.0	0.0	0.0	
320.0	90.0	-57.0							

Figure 55 b.   Sample Input Sheet (Cont.)

Card 3: Control Constants

Col. 1 & 2 - number of harmonics of rotational noise desired ($1 \leq N \leq 10$) (right adjusted)

Col. 4 - number of radial stations ($4 \leq N \leq 8$)

Col. 5-12 - angular increment of integration, degree (with decimal point)

(NOTE: $(360/\Delta\Psi)$ = even integer, $\Delta\Psi \geq \frac{1}{2}$ degree

Card 4: Output Controls

= 00 intermediate output not desired

= 99 intermediate output desired

Col. 1 & 2 - controls printout of input and radial integration

Col. 3 & 4 - controls printout of azimuthal integrations

Col. 5 & 6 - controls printout of S, β, u (from equation 26 of the report)

Card 5: Radial blade stations in fields of 9, inches*

For each radial station:

L_0 in Col. 1-8* on first card

$L_1 - L_{10}$ in fields of 8* on second card

$M_1 - M_{10}$ in fields of 8* on third card

For each field point:

One card with three parameters in fields of twelve, R, θ, σ, in that order (decimal points required).

*All fields specified must contain points.

89

Notes Regarding the Input Format

A case (Card 2, Col. 2) is a complete set of input data with a number of harmonics, fields points, etc. A new case would require a new title, a new set of basic constants, etc.

The number of field points here (Card 2, Col. 3 & 4) must agree with the number of cards describing the individual field points which are the last set of input cards.

The number of rotational noise harmonics desired (Card 3, Col. 1 & 2) partially determines the program running time.

The number of radial stations (Card 3, Col. 4) is arbitrary and is dependent on the number of stations at which blade loading is available. Evenly spaced stations over the length of the blade are desirable because the program interpolates between points. When the program is run at Sikorsky Aircraft, the last station is at the blade tip and the loading is zero at this position.

The angular increment of integration (Card 3, Col. 5-12) must be small to obtain a valid solution. If only one harmonic of rotational noise is to be calculated, an increment as large as 15 degrees may be used. When 10 harmonics of rotational noise are to be calculated, a maximum increment of 2 degrees is tolerable. Slightly increased accuracy may be gained by further reducing the increment, however, computer running time is increased accordingly.

The intermediate data printout which is determined by the output control card (Card 4) was used primarily for debugging the program. The normal printout includes the station number and radius, azimuth number and angle, section loading for each radial and azimuth position, field point coordinates, sound pressure and sound pressure level. The intermediate output adds a great deal of volume to the output and is not ordinarily required.

The number of radial blade stations (Card 5) must correspond to that specified in Card 3, Col. 4.

Description of Sample Case

The data for the sample 80-knot flyby case was taken from NASA TM X-952, "A Tabulation of Helicopter Rotor Blade Differential Pressures, Stresses, and Motions as Measured in Flight". The ship used was an H-34 (Sikorsky S-58) helicopter. Rotational noise was calculated for 5 harmonics of rotational noise from the main rotor at 11 field points.

The blade root pitch (β_0, β_1, $\overline{\beta_1}$) was taken from the pitch motion portion of Table 13(c) of the referenced NASA report. The harmonic loading for 7 blade stations was taken from Table 13(d) of the same report and the tip was considered the eighth station with zero loading assumed. The sample input and output for this case is shown in Figures 55 and 56, respectively.

Figure 56 a. Sample Output Sheet

Figure 56 b. Sample Output Sheet (Cont.)

Figure 56 c.   Sample Output Sheet (Cont.)

Figure 56 d.　Sample Output Sheet (Cont.)

80 KNOT CRUISE DATA S 58   NASA TM X-952 TABLE 13

FIELD POINT	RADIUS 0.320000E 03	AZIMUTH 0.900000E 02	ELEVATION -0.370000E 02
HARMONIC	SOUND PRESSURE	SPL	
1	0.019427852E-04	0.092301626E 02	
2	0.34729541E-04	0.81560021E 02	
3	0.76752042E-05	0.64539613E 02	
4	0.28992014E-05	0.59967596E 02	

Figure 56 e.   Sample Output Sheet (Cont.)

APPENDIX VII

SAMPLE CALCULATION-ASSUMED RELATIONSHIP BETWEEN BLADE LOADING, THRUST AND TORQUE

Referring to Figure 7, which shows an end view of a rotor blade, and replacing $\overrightarrow{q_m}$ with the steady force $\overrightarrow{F}$, note that

$$L = \frac{\overrightarrow{F}}{\Delta r}$$

where Δr is a spanwise element of blade. The in-plane force is then

$$F_i = L \, \Delta r \, \sin\beta$$

and the out-of-plane force is

$$F_o = L \, \Delta r \, \cos\beta$$

Thrust and torque are defined by

$$T = F_o \, n = nL \, \Delta r \, \cos\beta$$

$$Q = F_i \, rn = rnL \, \Delta r \, \sin\beta$$

From the relationships we find

$$\beta = \tan^{-1} \frac{Q}{rT}$$

$$L = \frac{T}{n \, \Delta r \, \cos\beta}$$

The values selected for the example are

Q = 7.79 x 10^5 pound-inches
T = 11,300 pounds
r = 269 inches
n = 4 blades
Δr = 7 inches

which give

β = 14.35 degrees
L = 417 pounds per inch

APPENDIX VIII

ROTATIONAL NOISE TEST INSTRUMENTATION

A block diagram of the instrumentation used in the Phase II test is presented in Figure 53. Measurements were made with a one-half-inch condenser microphone and the signal fed into the line input of a Nagra IIIB tape recorder. The 400-cps beeper signal used for a time reference was fed into the recorder through its microphone input and was generated by a General Radio transistorized oscillator. Overall levels were adjusted to avoid overloading the recorder. Data was recorded at hover, 40-knot, 80-knot, and 110-knot cruise, and 70-knot cyclic pullout. A recording was made with rotor system stopped and engine running to determine the extent of engine noise interference in the rotor noise frequency range of interest.

Figure 57. Rotational Noise Test Instrumentation

All noise records were analyzed twice. First, one-third-octave bandwidth plots of noise level versus frequency were made to determine the frequency of the main rotor blade passage and to evaluate masking noise. Second, plots were made of noise level versus time at the individual rotor harmonic frequencies as determined by the spectrum plots.

Frequency analysis of the records with the engine running and stopped rotor system showed that engine spikes appeared from 79 cps upward. The tail rotor fundamental blade passage frequency of the S-58 helicopter appears at 85 cps for the rotor speed used in the test. The fifth harmonic of the main rotor is at 75 cps and is masked by engine noise. For this reason, only the first four harmonics of the rotational noise were analyzed. This data is presented in the section entitled "Correlation of Measured and Calculated Rotational Noise".

98

APPENDIX IX

ROTOR SYSTEM PARAMETERS AND LOADS FOR PHASE III STUDY

The S-58 rotor system in the hover condition is used as the basis for the Phase III study of the effects of harmonic blade loading. The pertinent rotor system parameters are:

Number of blades	4
Blade radius, feet	28
Blade twist, degrees	-8
Blade chord, feet	1.367

Selected operating parameters are:

Rotor speed, rpm	210
Blade pitch angle at root, degrees	19.6
Thrust, pounds	11,300
Loaded radial increment, inches	7.0

Eight-tenths of the tip radius (r = 269 inches) is selected as the effective blade radius. The pitch angle β, corrected from the root angle for blade twist is 14.35 degrees.

Figure 58. Blade Aerodynamic Loading
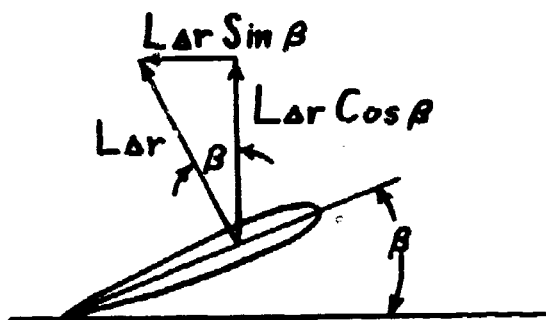
From Figure 58,

L = blade section loading, pounds per inch

r = loaded blade incremental radius, inches

β = blade pitch angle, degrees

n = number of blades

Total thrust $T = nL \, \Delta r \cos\beta$

or, solving for L,

$$L = \frac{T}{n \Delta r \cos\beta} = \frac{11,300}{4 \times 7 \times \cos 14.35°} = 417 \text{ pounds per in.}$$

This 417 pounds-per-inch blade loading is used as the steady component of all Phase III calculations. Harmonic loading levels are fractions of this figure.

99

DOCUMENT CONTROL DATA - R&D

(Security classification of title, body of abstract and indexing annotation must be entered when the overall report is classified)

1. ORIGINATING ACTIVITY (Corporate author)	2a. REPORT SECURITY CLASSIFICATION
Sikorsky Aircraft	Unclassified
Division of United Aircraft Corporation	2b. GROUP
Stratford, Connecticut	

3. REPORT TITLE

Helicopter Rotor Noise Generation and Propagation

4. DESCRIPTIVE NOTES (Type of report and inclusive dates)

Final Report

5. AUTHOR(S) (Last name, first name, initial)

Schlegel, Ronald G., King, Robert J., Mull, Harold R.

6. REPORT DATE	7a. TOTAL NO. OF PAGES	7b. NO. OF REFS
October 1966	115	34

8a. CONTRACT OR GRANT NO.	9a. ORIGINATOR'S REPORT NUMBER(S)
DA 44-177-AMC-141(T)	
b. PROJECT NO.	USAAVLABS Technical Report 66-4
Task 1P121401A14801	
c.	9b. OTHER REPORT NO(S) (Any other numbers that may be assigned this report)
d.	

10. AVAILABILITY/LIMITATION NOTICES

Distribution of this document is unlimited.

11. SUPPLEMENTARY NOTES	12. SPONSORING MILITARY ACTIVITY
	US Army Aviation Materiel Laboratories
	Fort Eustis, Virginia

13. ABSTRACT

An improved method is presented for calculating rotor system overall vortex noise and frequency spectra for stalled and unstalled rotors. Correlation of measured and predicted vortex noise was evaluated using two rotor systems operating over a wide range of speeds and thrusts. Correlation was found to be excellent. Blade tip planform studies revealed significant vortex noise reductions with tapered tips.

A new procedure is also derived for calculating near and far field rotor rotational noise with nonuniform inflow. The method extends the standard steady load method by including the effects of harmonic airloads. Correlation studies were conducted using an H-34 helicopter. Agreement between low frequency measured and predicted noise was good. However, correlation with high harmonic rotational noise was poor. This is probably due to inadequate definition of high harmonic airloads.

Presented results establish the importance of high harmonic rotational noise for detectability and loudness, and further work is recommended to more accurately define high harmonic blade loading. Since an airload measurement program is being conducted on the NH-3A, it is recommended that a correlation program be conducted to more fully evaluate the accuracy of the presented noise analysis program using the NH-3A airload results.

This study was performed for single rotor systems only, and in its present form is not directly applicable to systems with multiple rotors in juxtaposition.

DD FORM **1473** JAN 64

14. KEY WORDS	LINK A		LINK B		LINK C	
	ROLE	WT	ROLE	WT	ROLE	WT
Noise Helicopter Rotor Noise						

INSTRUCTIONS

1. ORIGINATING ACTIVITY: Enter the name and address of the contractor, subcontractor, grantee, Department of Defense activity or other organization *(corporate author)* issuing the report.

2a. REPORT SECURITY CLASSIFICATION: Enter the overall security classification of the report. Indicate whether "Restricted Data" is included. Marking is to be in accordance with appropriate security regulations.

2b. GROUP: Automatic downgrading is specified in DoD Directive 5200.10 and Armed Forces Industrial Manual. Enter the group number. Also, when applicable, show that optional markings have been used for Group 3 and Group 4 as authorized.

3. REPORT TITLE: Enter the complete report title in all capital letters. Titles in all cases should be unclassified. If a meaningful title cannot be selected without classification, show title classification in all capitals in parenthesis immediately following the title.

4. DESCRIPTIVE NOTES: If appropriate, enter the type of report, e.g., interim, progress, summary, annual, or final. Give the inclusive dates when a specific reporting period is covered.

5. AUTHOR(S): Enter the name(s) of author(s) as shown on or in the report. Enter last name, first name, middle initial. If military, show rank and branch of service. The name of the principal author is an absolute minimum requirement.

6. REPORT DATE: Enter the date of the report as day, month, year; or month, year. If more than one date appears on the report, use date of publication.

7a. TOTAL NUMBER OF PAGES: The total page count should follow normal pagination procedures, i.e., enter the number of pages containing information.

7b. NUMBER OF REFERENCES: Enter the total number of references cited in the report.

8a. CONTRACT OR GRANT NUMBER: If appropriate, enter the applicable number of the contract or grant under which the report was written.

8b, 8c, & 8d. PROJECT NUMBER: Enter the appropriate military department identification, such as project number, subproject number, system numbers, task number, etc.

9a. ORIGINATOR'S REPORT NUMBER(S): Enter the official report number by which the document will be identified and controlled by the originating activity. This number must be unique to this report.

9b. OTHER REPORT NUMBER(S): If the report has been assigned any other report numbers *(either by the originator or by the sponsor),* also enter this number(s).

10. AVAILABILITY/LIMITATION-NOTICES: Enter any limitations on further dissemination of the report, other than those imposed by security classification, using standard statements such as:

(1) "Qualified requesters may obtain copies of this report from DDC."

(2) "Foreign announcement and dissemination of this report by DDC is not authorized."

(3) "U. S. Government agencies may obtain copies of this report directly from DDC. Other qualified DDC users shall request through

_____."

(4) "U. S. military agencies may obtain copies of this report directly from DDC. Other qualified users shall request through

_____."

(5) "All distribution of this report is controlled. Qualified DDC users shall request through

_____."

If the report has been furnished to the Office of Technical Services, Department of Commerce, for sale to the public, indicate this fact and enter the price, if known.

11. SUPPLEMENTARY NOTES: Use for additional explanatory notes.

12. SPONSORING MILITARY ACTIVITY: Enter the name of the departmental project office or laboratory sponsoring *(paying for)* the research and development. Include address.

13. ABSTRACT: Enter an abstract giving a brief and factual summary of the document indicative of the report, even though it may also appear elsewhere in the body of the technical report. If additional space is required, a continuation sheet shall be attached.

It is highly desirable that the abstract of classified reports be unclassified. Each paragraph of the abstract shall end with an indication of the military security classification of the information in the paragraph, represented as *(TS), (S), (C),* or *(U).*

There is no limitation on the length of the abstract. However, the suggested length is from 150 to 225 words.

14. KEY WORDS: Key words are technically meaningful terms or short phrases that characterize a report and may be used as index entries for cataloging the report. Key words must be selected so that no security classification is required. Identifiers, such as equipment model designation, trade name, military project code name, geographic location, may be used as key words but will be followed by an indication of technical context. The assignment of links, rules, and weights is optional.